

Exospheres and Atmospheric Escape

**R.E. Johnson · M.R. Combi · J.L. Fox · W.-H. Ip ·
F. Leblanc · M.A. McGrath · V.I. Shematovich ·
D.F. Strobel · J.H. Waite Jr.**

Received: 28 February 2008 / Accepted: 7 July 2008 / Published online: 20 August 2008
© Springer Science+Business Media B.V. 2008

Abstract Aeronomy is a description of the physics and chemistry of the upper atmospheres and ionospheres of planetary bodies. In this chapter we consider those processes occurring

R.E. Johnson (✉)
Engineering Physics, University of Virginia, Charlottesville, VA 22904, USA
e-mail: rej@virginia.edu

R.E. Johnson
Physics Department, New York University, 4 Washington Pl., New York, NY 10003, USA

M.R. Combi
Department of Atmospheric, Oceanic and Space Sciences, University of Michigan, Ann Arbor,
MI 48109, USA
e-mail: mcombi@umich.edu

J.L. Fox
Physics Department, Wright State University, Dayton, OH 45435, USA
e-mail: Jane.Fox@wright.edu

W.-H. Ip
Institute of Astronomy, National Central University, Chung Li 32054, Taiwan
e-mail: wingip@astro.ncu.edu.tw

F. Leblanc
Service d'Aeronomie du CNRS, Paris, France
e-mail: francois.leblanc@aerov.jussieu.fr

F. Leblanc
Osservatorio Astronomico di Trieste, 34131 Trieste, France

M.A. McGrath
Marshall Space Flight Center, Huntsville, AL 35899, USA
e-mail: melissa.a.mcgrath@nasa.gov

V.I. Shematovich
Institute of Astronomy RAS, 48 Pyantnitskaya str., Moscow 119017, Russian Federation
e-mail: shematov@inasan.ru

in the upper atmosphere that determine the structure of the corona and lead to molecular escape.

Keywords Atmospheric escape · Planetary corona · Exobase · Exosphere

1 Introduction

Those processes occurring in the upper atmosphere of a planet or planetary satellite that determine the structure of the corona and lead to molecular escape are considered in this paper. A planet's atmosphere decreases in density with increasing altitude, thus an altitude is eventually reached above which molecules can travel planetary scale distances with a very small probability of making a collision. At such altitudes atoms or molecules that have energies greater than their gravitational binding energy can escape to space if their radial velocity is outward. This region of the atmosphere is called the exosphere or the planetary corona. The lower boundary for this region, called the exobase, is defined as that altitude where the atmospheric scale height, H , is about the same size as the mean free path for collisions, l_c . The Knudsen number, Kn , is the ratio between the mean free path and the density scale. It defines the transition region from a gas that is dominated by collisions and behaves like a fluid to a gas that should be modeled stochastically. Therefore, the exobase is also defined to occur where $Kn \sim 1$. In a gas of randomly moving molecules the mean free path for collisions is $l_c \approx 1/(\sqrt{2}\sigma n)$, where n is the molecular number density and σ is the *hard sphere cross section* which is independent of energy and assumes isotropic scattering. Therefore, setting $[\sigma n_{\text{exo}} H] \sim 1$ is often used to define the exobase. In this estimate the exobase occurs at a column density: $N(r_{\text{exo}}) \sim [n_{\text{exo}} H] \sim 1/\sigma$, where r_{exo} is the exobase radius; $\sigma \sim 1\text{--}3 \times 10^{-15} \text{ cm}^2$ is often used giving $N(r_{\text{exo}}) \sim 1\text{--}0.3 \times 10^{15} / \text{cm}^2$ (Chamberlain and Hunten 1987). On Mercury, the Moon, and many of the outer solar system icy bodies, the column of bound gas is less than $1/\sigma$, so that escape can occur from the physical surface.

The exobase is often used as the average altitude from which molecules escape to space. This is a crude approximation since hot atoms and molecules escape from depths well below the nominal exobase as seen in Fig. 1 for Titan's atmosphere. In addition, collisions involving atoms and molecules are energy dependent and dominated by forward scattering, so that hard sphere cross sections are a poor approximation and coronas often have molecular constituents. Finally, many of the processes that energize the exobase region reach a maximum well below the exobase, so that the structure of the exosphere is determined by the aeronomy occurring deep in the thermosphere requiring a description of the transport processes.

To more carefully define the nominal exobase, one needs to know the mean free path prior to a significant momentum transfer collision in an atmosphere that is not necessarily exponential. That is, an escaping hot particle can not suffer a momentum transfer collision that is sufficient to reduce its energy below the escape energy or to scatter it so that it is no longer moving upward. Using realistic potentials, a hot particle of energy E moving through

D.F. Strobel
Johns Hopkins University, Baltimore, MD 21218, USA
e-mail: dstrobel@jhu.edu

J.H. Waite Jr.
Southwest Research Institute, P.O. Drawer 28510, San Antonio, TX 78228, USA
e-mail: hwaite@swri.edu

a background of identical atoms or molecules [e.g., \sim eV O in an O thermosphere (Johnson et al. 2000)] is significantly deflected in an average distance $l_c \sim [bn\sigma_d]^{-1}$, where σ_d is the momentum transfer (diffusion) cross section. Here b is a number that depends weakly on the potential; for a steeply varying potential with forward scattering, $b \sim 0.5$ (Johnson 1990, 1994). Assuming hot recoils, or hot particles in the tail of a thermal distribution, moving upward at random angles, the escape probability from a depth r is

$$P_{\text{es}} = \exp\left(-\int_r^\infty ds/l_c \cos\theta\right) \approx \exp[-bn(r)\sigma_d/\cos\theta]. \quad (1a)$$

Here the integral is along the particle's trajectory, ds , θ is the direction of motion, assumed upward, and N is the integrated column density. Since the corona is often not a simple exponential, the average column for escape, N_{es} , should be used:

$$N_{\text{es}} \approx \left[\int_0^\infty dN \int_0^1 d\cos\theta N P_{\text{es}} \right] / \left[\int_0^\infty dN \int_0^1 d\cos\theta P_{\text{es}} \right] \approx c/\sigma_d^{-1}. \quad (1b)$$

Here $c \approx (2/3b)$ and the exobase altitude is obtained from $N(r_{\text{exo}}) \approx N_{\text{es}}$. Simulations and transport equations using realistic potentials give mean escape depths ($N_{\text{es}}\sigma_d$) ~ 1.3 (Johnson 1994, Appendix A). Detailed calculations of the O + O collision, averaging over the ground state multiplet (Kharchenko et al. 2000; Tully and Johnson 2001), give $\sigma_d = 1.3 \times 10^{-15}$ cm² for a 2 eV O moving in an O thermosphere or $N_{\text{es}} \sim 10^{15}$ O/cm². Since σ_d decreases slowly with increasing energy, N_{es} should be averaged over the hot particle energy distribution. It is usually evaluated at the escape energy, slightly underestimating N_{es} . Therefore, the exobase is not unique as it depends on the escaping molecule and its energy.

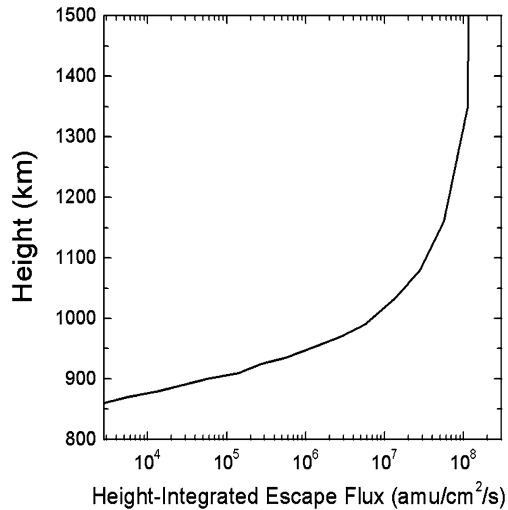
In the Chamberlain approximation for escape described in Sect. 2.1 below, only those atoms that are produced at or above the exobase with energies exceeding the escape energy and oriented upward are considered. However, using a single exobase altitude in a realistic atmosphere is problematic and misleading because it is different for different molecules and is an extended region. Therefore, this model provides only a rough prediction and computer simulations are now common, as described in Sects. 2.3 and 2.4. In the following we use models for the processes considered in the other papers in this issue to describe the physics and chemistry leading to the formation of a planetary corona and molecular escape. Results of simulations are then reviewed for a number of solar system bodies. Bodies with relatively robust atmospheres, for which escape is a relatively small effect at present, are first considered. This is followed by descriptions of icy bodies in the outer solar system for which escape can play a dominant role. The escaping molecules invariably leave a trail of neutral gas as is well known for comets. For a satellite orbiting a planet, this gas can remain gravitationally bound to the planet forming a nearly toroidal atmosphere. Since these atmospheres are extensions of the satellite exospheres and populate the planet's magnetosphere, they are discussed along with their source body.

2 Modeling of the Exosphere and Escape

2.1 Chamberlain Exobase Model

Chamberlain (1963) developed a widely used analytic model of the density of an exosphere. It is based on the assumptions that the speed distribution is Maxwellian at the exobase,

Fig. 1 Height-integrated mass escape flux due to photochemistry and atmospheric sputtering in the transition region of the Titan's upper atmosphere: most escaping molecules originate at altitudes below the nominal exobase (~ 1450 km) (adapted from: Schematovich et al. 2003). This flux at 1500 km ($\sim 1.2 \times 10^8$ amu/cm²/s) is about an order of magnitude smaller than recent estimates based on Cassini data (see Sect. 4.4), but the source region of hot particles is the same



that collisions can be ignored above the exobase, that the only force acting is the gravity, and that the speed distribution vs. altitude is obtained from the Liouville equation. Three populations of particles were considered: ballistic, satellite, and escaping. Using the Liouville equation, an analytical formula was derived for the density of each population above the exobase. This approach was generalized for a non-uniform exobase (Vidal-Madjar and Bertaux 1972) and a rotating planet (Hartle 1973; Kim and Son 2000; Kim et al. 2001). Velocity distributions produced by photo-dissociation and atmospheric sputtering have also been used. For instance, in order to fit the recent INMS/CASSINI measurement of Titan's exospheric density, De La Haye et al. (2007a) required an enhanced high energy tail to represent the hot particles produced below the exobase. The full distribution function was described by a kappa-distribution or a Maxwellian combined with a power-law distribution. A best fit was found for the corona densities over a narrow range of altitudes using a kappa distribution to account for both hot and thermal components.

Exospheres like Titan's, having a non-thermal component, require a description of the energizing processes below the exobase where collisions can not be neglected. Deviations from local thermal equilibrium start at $Kn \sim 0.1$, which occurs at 650 km in Titan's atmosphere. Therefore, production and transport of hot particles into the corona requires solving a Boltzmann equation or a Monte Carlo simulation as discussed below.

2.2 Boltzmann Transport

In the two stream approximation, the flux of hot particles in a background thermal atmosphere is derived from the full Boltzmann transport equation (Schunk and Nagy 2000). Dividing the flux into upward $\Phi^+(E, z)$ and downward $\Phi^-(E, z)$ components, where E is the kinetic energy and z the altitude, results in coupled linear equations that are solved for a range of altitudes up to the exobase. The velocity distribution for the hot particles at the exobase is $\{f(z, v) = [\Phi^+(E, z) + \Phi^-(E, z)]/v(E)\}$, where $v(E)$ is the speed corresponding to the kinetic energy E (Nagy and Banks 1970). The exospheric structure and escape is then determined using the Liouville equation. Nagy et al. (1981) modeled the first detection of hot O in Venus' exosphere produced by dissociative recombination of O_2^+ . They used branching ratios from Rohrbaugh and Nisbet (1973) to reproduce the O scale height but

over estimated the density. This was subsequently corrected using better input parameters (Nagy and Cravens 1988; Nagy et al. 1990). Measured branching ratios for dissociative recombination (Kella et al. 1997) and the vibrational distribution of the O_2^+ were used by Kim et al. (1998) for solar minimum and maximum conditions at Mars. The role of CO^+ dissociative recombination and photo-dissociation of the CO molecules at Mars' was calculated similarly (Nagy et al. 2001).

Solutions have been developed for a linearized Boltzmann equation in order to describe gas flow in the transition region (Shizgal and Lindenfeld 1982; Shizgal and Blackmore 1986; Shizgal and Arkos 1996; Shizgal 1999). This approximation is used to describe the flow of hot or minor species through the background atmosphere assuming their effect is negligible (Shematovich et al. 1994). Kabin and Shizgal (2002) calculated the Boltzmann collisional term for endogenic or exothermic reactions between species that both have Maxwellian distributions and scatter isotropically. Their results were successfully compared with Monte Carlo test particle simulations described below. They derived the distribution of hot O in the Venusian and Martian atmospheres produced by dissociative recombination of O_2^+ including collisions with thermal O. Pierrard (2003) also solved a linearized Boltzmann equation using a spectral method to determine the flux of H and He through an atmospheric background.

2.3 Monte Carlo Simulations

The Direct Simulation Monte Carlo (DSMC) model is a stochastic method used to describe a rarefied gas and is equivalent to solving the Boltzmann equation. It treats both the dynamic and stochastic nature of the gas (Bird 1994) and is valid if the collisions are statistically independent, multi-particle collisions are negligible, and the collision time is short compared to the time between collisions. All types of collisions can be accounted for including those between atmospheric particles, so that the non-linear processes can be included (Shematovich et al. 1994, 1999, 2005a, 2005b; Krestyanikova and Shematovich 2005, 2006). Each species is described in term of its phase space distribution. The motions of representative particles, each assigned a weight, are followed taking into account collisions and forces. Source distributions and collisions are typically treated using Monte Carlo models. DSMC is time consuming when the domain is highly collisional, but is useful for describing the transition from the collisional to collisionless regime (Marconi et al. 1996). It has been used to simulate heating of the exobase region, the coronal structure, and escape using knowledge of the processes that produce hot atoms and molecules. DSMC simulations have been applied to the exobase region of Mars (Leblanc and Johnson 2001; Krestyanikova and Shematovich 2005, 2006), Titan (Shematovich et al. 2003; Michael and Johnson 2005), and Europa (Shematovich et al. 2005b) as well as to a comet's coma (Combi 1996).

Simplifications are often used, because large numbers of particles are needed to obtain an accurate speed distribution. The velocity space is often divided into a hot particle population (the tail of the distribution) and a thermal background. Test particle simulations track the hot component or trace species allowing collisions only with the background gas and are equivalent to solving a linearized Boltzmann equation. Such simulations have been extensively used at the Earth to model the escape and exospheric formation of minor species (Chamberlain and Campbell 1967; Chamberlain 1969; Barakat and Lemaire 1990; Hodges 1994). These simulations have also been tested against a multi-moment solution (Demars et al. 1993) or a direct solution of the linearized Boltzmann equation (Shizgal and Blackmore 1986). Since the hot particles heat the thermosphere, adding a hot tail to a Maxwellian can be incorrect (Johnson et al. 2000).

1D test particle simulations were also used to describe the O exosphere at Mars produced by dissociative recombination of O_2^+ for different solar conditions (Ip 1988, 1990; Lammer

and Bauer 1991). Instead of the standard hard sphere cross sections, Johnson et al. (2000) used the, so-called, universal interaction potential (Ziegler et al. 1985) to describe O + O collisions in an O thermosphere and corona. They showed the escape rates obtained using test particle simulations compared favorably with DSMC results using the same potentials, but differed from hard sphere results. Hodges (2000) developed the first 3D model of the hot O component at Venus and Mars using realistic atmospheric and ionospheric models, but described the thermalization of the hot O by hard sphere collisions. 3D test particle simulations including realistic collision models were used to describe the structure of the exosphere induced by pick-up ion sputtering of Mars (Leblanc and Johnson 2001) and Titan (Michael et al. 2005). In a 1D simulation, (Leblanc and Johnson 2002a) described the effect on atmospheric sputtering of having molecular rather than atomic species at the exobase. They introduced a molecular dynamics collision code which accurately calculated the production of hot neutrals by collisional dissociation (Johnson et al. 2002). Chaufray et al. (2007) used a simpler model for Mars atmosphere, but took into account the dependence of the recombination rate on the solar zenith angle *and* self-consistently coupled the atmosphere simulation to a 3D hybrid simulation of the interaction with the solar wind (Modolo et al. 2005).

Monte Carlo simulations have rapidly increased in complexity and can be more useful than the Boltzmann equation when there are multiple species. The simpler test particle methods are sufficient unless the response of the atmosphere is needed. In addition, test particle methods below the exobase can be coupled to DSMC models in the exobase region and above. However, when the heating rate near the exobase is large accurate representation of the full speed distribution throughout the transition region requires an extensive, often intractable, computational effort in both the Monte Carlo and Boltzmann models. In addition, accurate cross sections are often not available, especially for collisions involving hot particles. Results of simulations for a number of planetary bodies will be described below.

2.4 Exosphere–Plasma Interactions

Since the incident plasma can be an important source of heating and atmospheric loss (Johnson and Luhmann 1998), the principal uncertainty in describing the atmosphere near the exobase is the description of the flow of the ambient and locally produced plasma through the corona.

The effect of a neutral exosphere on the formation of the magnetospheric bow shock and magnetic barrier has been discussed since Pioneer Venus and Mars Global Surveyor observations. The bow shock position at Venus was observed to move away from the planet with increasing solar activity (Alexander and Russell 1985), whereas no significant variation of the bow shock and magnetic pile-up boundary position was observed at Mars (Vignes et al. 2000). Bauske et al. (1998) and Kallio et al. (1998) used 3D single-fluid MHD models, in which a source term was introduced to account for the planetary ions, in order to evaluate the role of the exosphere on the bow shock position, and, hence, on the plasma flow (Ledvina et al. 2008). They concluded that the variations in the bow shock in going from solar minimum to maximum could be reproduced. Ma et al. (2002) and Modolo et al. (2005) used 3D MHD and hybrid models respectively, but did not find any significant dependence of the bow shock position on the exosphere structure at Mars even if an unrealistically high value of the photoionization rate was used. Unlike at Venus, these results emphasize the difficulty at Mars of inferring exospheric structure from bow shock position, contrary to the conclusion of Kotova et al. (1997).

Pérez-de-Tejada (1987, 1998), Lundin et al. (1991), Lundin and Dubinin (1992) calculated the atmospheric escape rate from weakly magnetized planets using the upstream

and downstream characteristics of the solar wind. They described the momentum transfer between the incident solar wind and the accelerated plasma by a simple relation using a coefficient for the scavenging efficiency (Lundin and Dubinin 1992). The cross section of the interaction region is defined to be between the mass loading boundary and the magnetopause (Lundin et al. 1991; Lundin and Dubinin 1992). The main difficulty is the lack of constraints on both the efficiency of the momentum transfer and the size of the transfer region. Luhmann et al. (1992) pointed out that this does not allow the use of present-day results to describe the history of the planet-solar wind interaction. Discussion of the interaction for the individual objects is given below.

3 Escape processes

3.1 Thermal Escape

Planetary and satellite atmospheres are confined by gravity. This is often characterized by the so-called Jeans parameter, λ : $\lambda = v_{\text{esc}}^2/U^2$, where $U = (2kT/m)^{0.5}$ is the most probable speed at temperature T , and $v_{\text{esc}} = (2GM/r_{\text{exo}})^{0.5}$ is the escape speed at the exobase. Larger values of λ imply a more tightly constrained atmosphere, as is evident by writing the exobase value of λ

$$\lambda \equiv \frac{GMm}{kTr_{\text{exo}}} \left[= \frac{\text{gravitational potential energy}}{\text{random kinetic energy}} \right] = \frac{r_{\text{exo}}}{H}.$$

As written, m is the mean molecular mass, $g = GM/r^2$ is the gravitational acceleration of an object of mass M , G is the gravitational constant, and the atmospheric scale height is $H = (kT/mg)$ all defined at the exobase. As discussed above, in region where l_c is much less than the local scale height, H ($\text{Kn} \approx l_c/H \ll 1$), the atmosphere can be treated as a fluid and the exobase is at $\text{Kn} \approx 1$. The transition from collision dominated ($\text{Kn} \ll 1$) to the quasi-collisionless exosphere ($\text{Kn} > 1$) is gradual, not abrupt, as discussed. For example, at Titan the ‘exobase region’ may be ~ 1000 km thick as the atmosphere transitions from N_2 to H_2 domination. While it is often stated that the fluid equations break down at the exobase, they are the first three moments of Boltzmann’s equation, so that, with care, they can be applied above the nominal exobase.

3.1.1 Jeans Escape—Thermal Evaporation

An ideal gravitationally bound atmosphere is one in which the escape rate is zero: $\lambda \rightarrow \infty$. Although this limit is unattainable, it is instructive. The classic model with no *bulk* outflow is that of Chamberlain, described above, in which escape is due to the fraction of upward moving atoms/molecules with velocities exceeding v_{esc} at the exobase. This gives the Jeans formula for thermal evaporation

$$F_{\text{Jeans}}(r_{\text{exo}}) = \frac{n(r_{\text{exo}})U}{2\sqrt{\pi}} (\lambda + 1)e^{-\lambda} \quad (1)$$

where λ is evaluated at the exobase. Since the tail of the Maxwellian distribution is depleted by escaping particles, it assumed to be rapidly replenished by collisions. In the Jeans limit, $\lambda \rightarrow 0$, the atmosphere is no longer bound and blows away with a flux $= n(r_{\text{exo}})v_{\text{ther}}/4$ where $v_{\text{ther}} = (8kT/\pi m)^{0.5}$. This is the upward directed thermally driven flux at the exobase and is used to describe the coma of a comet discussed later in this chapter. In the limit of

large λ , the atmosphere is gravitationally retained and Jeans escape is negligible. In the solar system, bodies with values of $\lambda \lesssim 50$ at the exobase have extended atmospheres and large values of $r_{\text{exo}}/r_p \geq 1.2$, where r_p is the planet radius (Strobel 2002). Some representative values of λ are: Pluto, $\lambda \sim 20\text{--}25$ at $r = 1450$ km and ~ 10 at the exobase ~ 4400 km, Titan, $\lambda \sim 55\text{--}60$ at $r = 3300$ km and ~ 45 at the exobase ~ 4300 km, Earth, $\lambda \sim 1000$ at $z = 85$ km and ~ 130 at the exobase ~ 500 km (but highly variable with solar activity), and Jupiter, $\lambda \sim 1860$ at $z = 350$ km and ~ 430 at the exobase $z \sim 2300$ km. The respective values of λ for Venus, Mars, Saturn, Uranus, and Neptune are 1600, 490, 1300, 200, and 450 at the 1 μbar level, whereas at their respective exobases: $\lambda \sim 350$ at $z = 140$ km, 200 at 160 km, 420 at 2500 km, 50 at 4700 km, 120 at 2200 km (cf. Strobel 2002). For comparison, the solar wind with a coronal temperature of 2×10^6 K, has $\lambda \sim 4$.

3.1.2 Hydrodynamic Escape

In contrast to Jeans escape, hydrodynamic escape is an organized outflow with a bulk velocity driven by the heating of the atmosphere. In steady state, with no net production or loss, the atmosphere below the exobase is described by the Euler equations for a pressure driven fluid (e.g., Landau and Lifshitz 1987). For 1D radial flow with velocity, v , the continuity, momentum and energy conservation equations can be written:

$$\frac{1}{r^2} \frac{\partial}{\partial r} (r^2 \rho v) = 0 \tag{2}$$

$$\frac{\partial}{\partial r} \left(\frac{1}{2} v^2 \right) + \frac{1}{\rho} \frac{\partial p}{\partial r} + \frac{GM}{r^2} = 0 \tag{3}$$

$$\frac{1}{r^2} \frac{\partial}{\partial r} \left[r^2 \left\{ \rho v \left(\frac{1}{2} v^2 + \tilde{c}_p T + \Phi_g \right) - \kappa \frac{\partial T}{\partial r} \right\} \right] = Q \tag{4}$$

where the viscous terms, which are important for substantial velocities, are ignored. Here ρ ($= mn$) is the mass density, v the bulk velocity, $[\tilde{c}_p T]$ the enthalpy with \tilde{c}_p the specific heat at constant p , Q the heating/cooling, κ [$= \kappa_0 (T/T_0)^s$] the thermal conductivity, and gravity is written as a potential Φ_g : $-\nabla \Phi_g = -GM \vec{r} / r^3$. Equation (2) gives the mass loss rate, written as $4\pi (mF) = [4\pi \rho v r^2]$.

Although one can analyze the importance of the various terms directly, these equations are often written using non-dimensional variables (e.g., Watson et al. 1981):

$$\lambda = \frac{GMm}{rkT_0}, \quad \tau = \frac{T}{T_0}, \quad \psi = \frac{mv^2}{kT_0} = \left(\frac{v}{c} \right)^2, \quad \zeta = \frac{Fk}{\kappa_0 r \lambda_0}, \quad c_p = \frac{\tilde{c}_p}{k/m} \tag{5}$$

Here $c = (kT_0/m)^{1/2}$ is the speed of sound, $s = 0$ in the expression for $\kappa(T)$, and subscript “0” denotes values at the lower boundary. The steady-state equations are then

$$\frac{d}{d\lambda} \left(\frac{1}{2} \psi \right) + \frac{1}{n} \frac{d(n\tau)}{d\lambda} - 1 = 0 \tag{6}$$

$$\frac{d}{d\lambda} \left(\lambda - c_p \tau - \frac{1}{2} \psi - \frac{\tau^s}{\zeta} \frac{d\tau}{d\lambda} \right) = \frac{(r_0 \lambda_0)^3}{\lambda^4} \frac{Q(n(\lambda, \mu_i))}{FkT_0} \tag{7}$$

where Q is a function of n and the mixing ratios of radiatively active constituents, μ_i .

Hydrodynamic escape is formulated in the high density approximation (Parker 1964; McNutt 1989) in which the gravitational potential is deep. Below the exobase the hydrodynamic expansion is slow, $v \ll c$, such that the gravitational energy is greater than the thermal energy and much larger than the flow energy: i.e., $\lambda \geq c_p \tau \gg \psi$. In this case the equations reduce to

$$\frac{d[\ln(n\tau)]}{d\lambda} - \frac{1}{\tau} = 0 \tag{8}$$

$$\frac{d}{d\lambda} \left(\lambda - c_p \tau - \frac{1}{\zeta} \frac{d\tau}{d\lambda} \right) = \frac{(r_0 \lambda_0)^3}{\lambda^4} \frac{Q(n(\lambda))}{FkT_0}. \tag{9}$$

Equation (8) is equivalent to (3) neglecting the flow term, resulting in an atmosphere in hydrostatic equilibrium. Equation (9), the scaled energy equation, also neglects the flow term in (4). Therefore, v must be small up to the exobase of the major constituent. The best measurements applicable to planetary escape are the Cassini INMS data for Titan’s upper atmosphere and exosphere. Fluid models calibrated to this data assume the flow goes supersonic for the light species, H₂ and CH₄, in an extended region above the exobase of the major constituent N₂ (Cui et al. 2008; Yelle et al. 2008; Strobel 2008a). The relevant asymptotic boundary conditions are n and $\tau \rightarrow 0$ as $r \rightarrow \infty$ (Parker 1964). Integration of (9) from the lower boundary to $r \rightarrow \infty$ ($\lambda \rightarrow 0$) yields

$$\lambda_0 = \int_0^{\lambda_0} \frac{(r_0 \lambda_0)^3}{\lambda^4} \frac{Q(n(\tau, \lambda))}{FkT_0} d\lambda + \left[c_p \tau + \frac{\tau^s}{\zeta} \frac{d\tau}{d\lambda} \right]_{\lambda_0}. \tag{10}$$

In (10) three processes drive the expansion. If the atmosphere is optically thin to EUV and UV radiation and the interaction with the plasma is negligible, the first term on the right is small. If also the heat conduction is small, then the dominant term on the right is $c_p \tau$ (the internal heat in (4)), plus $\frac{1}{2} \psi$ from (7) which was neglected in (10). Hence, $\lambda_0 \sim [c_p \tau + \frac{1}{2} \psi]$ {i.e., $mgr_0 \sim \tilde{c}_p T + mv^2/2$ } with $\tau \approx 1$ {i.e., $T \sim T_0$ } due to negligible heating. Ignoring the enthalpy, the atmosphere is traditionally defined to be in a blowoff if $\lambda < \frac{1}{2} \psi$ at the exobase [i.e., $v(r_{\text{exo}}) > v_{\text{esc}}$]. However, $c_p \sim 5/2$ and $7/2$ for atoms and diatomic molecules, respectively, and cannot be ignored. In this limit v is not negligible compared to c , so that ψ must be included in (10). For a vanishingly small total energy flux at infinity, $\lambda_0 \sim c_p + \psi/2$. More likely, the energy flux at infinity is finite and (10) does not apply. This blowoff condition is similar to the jets emitted from the surface of a comet, where $\lambda \ll 1$, and represents chaotic escape.

In contrast, slow hydrodynamic escape refers to an organized, controlled expansion of the atmosphere driven by net heating and upward thermal conduction through some boundary below which heating occurs. Hydrodynamic expansion can be driven by solar heating and escape is limited by the net heating rate (power absorbed times heating efficiency minus radiative cooling) (Hunten and Watson 1982). Therefore, the first term on the right of (10) dominates, so that, in the absence of thermal conduction, $\{[GMm/r_0](4\pi F)\} \approx \int_{r_0}^{\infty} Q4\pi r^2 dr$. This gives an upper limit to the mass escape flux by equating the gravitational energy per unit time that would be carried off by the escaping particles to the heating rate. To compare to Jeans escape, assume that the sonic point occurs at the exobase so that the outflow velocity, v , equals c (the isothermal speed of sound). Then $v = v_{\text{esc}}$ if $\lambda = 1/2$ at the exobase. This can be compared with the mean velocity of Jeans escape, $0.36v_{\text{esc}}$ [from (1) with $\lambda = 1/2$], giving the well known discrepancy of about a factor of three between bulk outflow escape and Jeans escape.

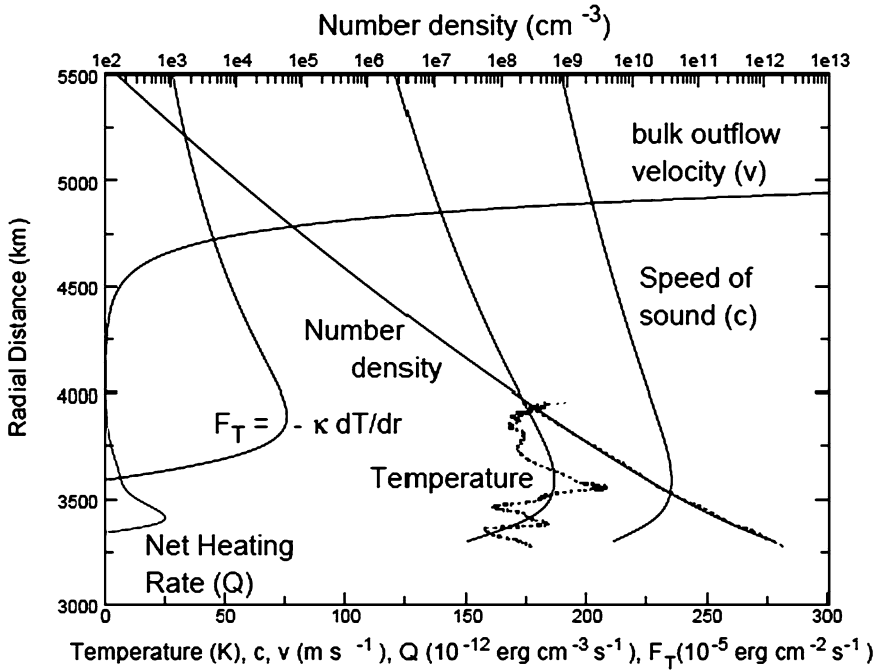


Fig. 2 A model for Titan’s atmosphere (Strobel 2008a): n , T , c , v , and upward thermal heat conduction flux (solid lines) for an N_2 atmosphere with solar medium conditions: net heating due mostly to CH_4 UV heating above the lower boundary at $r_0 = 3300$ km, $T_0 = 158$ K, and downward thermal heat conduction flux at lower boundary $= 4.0 \times 10^{-3}$ erg/cm²/s. Comparison with the HASI measurements of total number density and temperature (dashed lines) at $\sim 10.3^\circ S$ latitude. Assuming the model applies above the nominal exobase (here taken to be 4300 km), the low speed solution (Mach number < 0.3) is valid only to ~ 4750 km and the mass escape rate is 4.5×10^{28} amu/s

Equations (8) and (9) can be solved quasi-analytically if solar heating is represented by a δ function (McNutt 1989; Krasnopolsky 1999). They can also be solved numerically with distributed heating functions (Strobel 2008a, 2008b; for Titan and Pluto discussed below). These solutions were restricted to $\psi \ll 1$ ($v \ll c$) below the exobase. Tian and Toon (2005) solved Euler’s equations using distributed heating for Pluto’s atmosphere. Although they only included EUV absorption by N_2 , omitting the larger UV component absorbed by CH_4 , they obtained an order of magnitude larger escape rate than Krasnopolsky (1999) and Strobel (2008b).

For slow hydrodynamic expansion, the physics is as follows. Adiabatic cooling is assumed to occur throughout the atmosphere associated with the bulk outflow velocity in Fig. 2. This outflow can be driven by EUV/UV heating as in the model for Titan. There are also regions of net cooling due to IR emissions that locally exceed solar heating: above 3440 km in Fig. 2. Thermal heat conduction redistributes the heat, producing a temperature maximum at some altitude, below which a downward thermal heat conduction flux adjusts to both adiabatic and radiative cooling. Above the maximum, upward thermal conduction delivers power to sustain an expansion. At levels much above the temperature maximum, heat conduction must be about equal to what is needed to power the upward flow of mass in the model in Fig. 2. Solar heating near the exobase contributes only $\sim 10^{-3}$ of the heat conduction flux and plasma-induced heating is ignored.

Solutions below the exobase must be matched to an escape model, about which there is still controversy. In the model in Fig. 2 it is essential that heat conduction continues to collisionally power the expansion above the exobase until the flow speed exceeds the escape speed. The description of upward heat conduction in the exobase region has been estimated by a 13-moment expansion of the Boltzmann equation, since the fluid is not Maxwellian. In such a model heat conduction is thought to redistribute velocities into an upwardly directed, enhanced tail augmenting escape, as proposed for H₂ escape from a nitrogen atmosphere (Cui et al. 2008). Thus there can be an intimate link between a perturbed velocity distribution and hydrodynamic escape. The expansion below is powered by the delivery of heat from the region of maximum heating to higher altitudes by thermal heat conduction, which requires a decreasing temperature profile. In the above model, hydrodynamic expansion with an upward thermal heat flux and the collisional production of a high speed tail beyond the escape velocity due to heat conduction into the exosphere are two descriptions of the same phenomenon. However, whether or not, for a given λ , the distortion in the tail of the velocity distribution produced by thermal conduction is sufficient to produce the required escape flux has not been demonstrated computationally.

3.2 Photochemical-Induced Escape

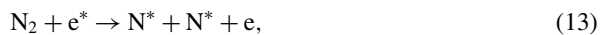
Photochemical escape has its origin in the interaction of solar photons with neutrals in the upper thermosphere and exosphere. This includes direct interactions of photons and photoelectrons with thermospheric molecules, as well as chemical reactions of ions with neutrals and electrons. Direct excitation includes photodissociation, e.g.,



(Brinkmann 1971; Fox and Bakalian 2001); photodissociative ionization, e.g.,



(McElroy et al. 1977; Fox and Dalgarno 1983); photoelectron-impact dissociation, e.g.,



(McElroy et al. 1977; Fox 1993); and photoelectron-impact dissociative ionization, e.g.,



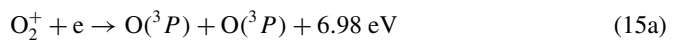
(Fox and Dalgarno 1983). The asterisks denote electronic excitation or a particle with excess kinetic energy, for neutrals the so-called hot particles. The energy released in (11) is the difference between the photon energy and the molecular dissociation energy, which can be reduced by electronic excitation of the products. Electron impact dissociation of CO primarily produces two ground state atoms (Cosby 1993). Because the interaction of photons and electrons with neutrals is not the same, this assumption should only be adopted when there is no detailed information about the individual process. Thus our ability to determine the energy released depends on knowledge of the branching ratios of the various channels, information that is often not available.

The computation of escape rates due to photodissociation is also affected by the lack of cross sections, which are usually assumed to be equal to the difference between the photoabsorption and photoionization cross sections. Unfortunately, these cross sections are

often not measured simultaneously and much of the time they are taken from different sources (Huestis et al. 2008). In addition, photodissociation of many atmospherically important molecules, such as CO, CO₂, H₂ and N₂, proceeds by absorption into discrete states followed by predissociation (Fox and Black 1989; Fox 2007). In such cases, the photoabsorption cross sections must be measured at very high resolution, on the order of 10⁻⁴ nm, and combined with similarly high resolution solar fluxes in order to compute the dissociation rates and product energies. Fox and Black (1989) constructed such cross sections and solar fluxes for CO and applied the results to Venus. Measurements and calculations of very high resolution cross sections for N₂ (e.g., Stark et al. 2007; Sprengers et al. 2005; Lewis et al. 2005), and CO₂ have been carried out by several groups (Huestis et al. 2008), but are generally not available over the entire energy range of interest.

In photoelectron impact dissociation (13), the excess energy is usually carried away by the electron. The energies of the products are estimated by measurements of appearance potentials or time-of-flight measurements (e.g., Armenante et al. 1985), or by analysis of Doppler-broadened lineshapes. Ajello and Ciocca (1996) analyzed the line shapes of the NI emissions at 1200 Å due to 30 eV electrons on N₂ and found that the excited N(⁴P) atoms produced were translationally hot, with average energies ~ 1 eV. Prokop and Zipf (1982) found that the average energy of the N produced in electron impact dissociation of N₂ was ~ 0.45 eV. Fox and Dalgarno (1979) concluded that in electron impact dissociation of CO₂ the mean energy released was ~ 1 eV. Dissociative ionization, processes (12) and (14), are known to produce very energetic products (e.g., Loch and Davister 1995; Tian and Vidal 1998). The energetic ions and neutrals are mostly due to predissociation of electronically excited states of the ions. This is also the case for the energy release when a fast proton produces dissociative charge exchange in N₂ (Luna et al. 2003) and O₂ (Luna et al. 2005). The fraction of atoms with the escape energy must be estimated from such measurements.

Exothermic reactions among the ions, neutrals and electrons near the exobase produce translationally hot species. Dissociative recombination (DR) of molecular ions is one of the most exothermic reactions. DR of O₂⁺ is known to be the photochemical source of escaping O from Mars as discussed below. It also is a major source of the hot O in coronas on Earth (Shematovich et al. 1994; Bisikalo et al. 1995), and Venus, also described below. Starting with O₂⁺ vibrational ground state, the reaction proceeds via five channels with different exothermicity:



The branching ratios have been measured in ion storage rings and are found to be 0.22, 0.42, 0.0, 0.31, and 0.05, respectively (Kella et al. 1997). Peverall et al. (2001) have also measured branching ratios for the channels of DR of O₂⁺ as a function of energy and a negligible yield for (15c) is predicted (Guberman and Giusti-Suzor 1991). Since the escape energy for O at the Martian exobase is ~ 1.98 eV, only O produced via (15a) and (15b) can escape. The exothermicities are increased by vibrational excitation of the O₂⁺ (*v* > 0). Vibrational distributions of O₂⁺ in the atmospheres of Earth and Venus have been calculated (Fox 1985, 1986) as have the O energy spectra at the exobases of the terrestrial planets (Fox and Hač

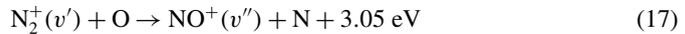
1997a, 1997b). O_2^+ is predicted to be significantly vibrationally excited at the exobases on all three planets.

Branching ratios for the various energetically allowed channels for dissociative recombination have been measured for N_2^+ (Kella et al. 1997; Peterson et al. 1998) and for CO^+ (Rosen et al. 1998). For DR of CO_2^+



Siersen et al. (2003) found the branching ratio for (16a) was about 9%. This was questioned by Viggiano et al. (2005) who found that nearly all the reactions proceeded by (16a).

Other exothermic ion–molecule reactions can also produce escape: e.g.



(Fox and Dalgarno 1983; Fox 1993). In the center of mass frame, 68% of the exothermicity is carried away by the N atom. The absolute value of the exothermicity is increased by vibrational excitation of N_2^+ and reduced by vibrational excitation of the NO^+ . The radiation rate by vibrational-rotational transitions of N_2^+ is small, so that it will be vibrationally excited near and above the Martian exobase (Fox and Hać 1997b). The vibrational distribution was computed for the ionospheres of the Earth (Fox and Dalgarno 1985) and Venus. If we assume that the energy released in (17) is distributed statistically among the vibrational, rotational, and translational modes, with $N_2^+(v = 0)$ in the vibrational ground state, 31% of the product energy appears as vibrational energy, correspondingly reducing the escape probability.

The non-thermal escape of N_2 , CH_4 , H, H_2 , N, NH, HCN, CN and small hydrocarbons has been studied by Cravens et al. (1997) and by De La Haye et al. (2007b). Cravens et al. computed the escape rate for 19 species and 47 processes, including dissociative recombination of ions, ion-molecule reactions, electron-impact dissociative and dissociative ionization of molecular ions. To obtain the escape fluxes, they integrated the production profiles from the exobase to 2500 km. De La Haye et al. (2007b) included only 12 species, but used the 2-stream approximation to compute the escape rates of these ions through a background mixture of N_2 , CH_4 , and H_2 . They estimated the photochemical escape rates of N and C ions in all forms as $8.3 \times 10^{-24} \text{ s}^{-1}$ and $7.2 \times 10^{24} \text{ s}^{-1}$ respectively.

3.3 Plasma-Induced Escape

For a magnetized planet, the intrinsic field is a natural shield for the atmosphere, and part of the apparent ion loss is recycled by the fields as shown for the Earth (Seki et al. 2001). If the planetary body has a relatively strong magnetic field that can interact with either the solar interplanetary magnetic field or the field of a parent body, such as the magnetospheres of Saturn and Jupiter interacting with the solar wind and the field of Ganymede interacting with the Jovian plasma, then magnetic reconnection processes occur leading to the loss of a body's ionosphere. If the body is weakly or non-magnetized, the morphology of the induced fields and the position exosphere along with the scale lengths for interaction, such as the mean free path and the ion gyroradius, will determine the nature of loss processes.

Ionization in the exosphere and upper atmosphere can lead to *ion loss* as well as the formation of energetic neutral *atoms* (ENAs) by charge exchange. The polar wind (Axford 1968) at the Earth is an example of an ion loss process. The interaction with the solar wind modifies the magnetic field configuration close to the Earth, compressing the field on the

sunward side and forming a tail on the anti-sunward side. At high latitudes thermal plasma from the polar ionosphere can flow into the magnetosphere and down the tail resulting in the loss of H^+ , He^+ and O^+ . Processes similar to this occur on non-magnetized planetary bodies Venus and Mars, as discussed later, resulting in day to night flow down the tail (e.g., Shinagawa and Cravens 1989; Ma and Nagy 2007).

The principal ionization processes are photo-ionization, ionization by electronic impact, and charge exchange. Charge exchange has been studied as a principal source of non-thermal escape of H atoms at the Earth (Shizgal and Arkos 1996), Venus (Hodges 1993) and Mars (Nagy et al. 1990) leading to the high D/H ratio measured in Venus' atmosphere (Donahue et al. 1982). Charge exchange production of ENAs is usually considered as a nearly resonant collision, equivalent to the exchange of an electron without significant momentum transfer (Shizgal and Lindenfeld 1982; Shizgal and Arkos 1996). Kallio et al. (1997) showed that at Mars the region where ENAs are formed by charge exchange between solar wind H^+ and exospheric O occurs on the dayside in a thin layer whose size depends on solar activity. This has been directly observed by ASPERA 3 on Mars Express (Gunell et al. 2006). Zhang et al. (1993) studied the roles of photo-ionization, charge exchange and impact ionization at Mars and Venus, and concluded that the dominant ionization mechanism is electron impact, but was criticized by Krymskii and Breus (1996, see reply by Luhmann 1996). Using their electric and magnetic field model, Kallio and Koskinen (1999) developed a test particle simulation based on an exospheric model (Nagy et al. 1990) in order to describe the ionization of exospheric O and the escape of O^+ ions at Mars. They concluded that ions formed in the exosphere can produce the loss rate measured by Lundin et al. (1989). Ma and Nagy (2007) found that the O^+ escape rate decreases by a factor 3 when photo-ionization and electron impact ionization rates are set to zero, confirming that the escaping O^+ are formed above the Martian exobase. Cravens et al. (2002) used a test particle MHD model to simulate pick-up ion trajectories and reproduced the 55–72 keV ion population reported by Phobos 2 (McKenna-Lawlor et al. 1993).

A fraction of the pick-up ions and ENAs can re-impact the atmosphere with enough energy to induce heating and atmospheric sputtering. This is particularly true when the pick-up ion gyroradius is of the order of the planet radius, as at Mars and Venus for O^+ . The sputtering efficiency is given by a yield, Y . It is the ratio between the number of escaping particles and the number of incident particles and varies inversely with the planet's gravitational energy (Johnson 1990). Sputtering of an atmosphere can occur by direct scattering of atmospheric molecules, also called knock-on, which dominates at grazing incidence by incident light ions or ENAs with energies $\sim keV$: $Y \lesssim 1$. For heavy incident ions, a cascade of recoils is set in motion with some having sufficient energies and the appropriate direction of motion to escape: $Y \gtrsim 1$ (Johnson 1994). This occurs when keV to few 100 keV incident O^+ pickup ions and ENAs impact the atmospheres of Mars and Venus (Johnson et al. 2000) or when molecular pick-up ions re-impact Titan's atmosphere (Michael et al. 2005).

Watson et al. (1980) showed that atmospheric sputtering of Mars and Venus by impacting solar wind protons was inefficient. Subsequently Luhmann and Kozyra (1991) calculated the flux of re-impacting pick-up ions and ENAs using a 1D exospheric model of the O density and the solar wind flow derived from a gas-dynamic model. They concluded that a significant number of sputtered O should escape from Mars and Venus. Because the sputtered products add to the exosphere they can in turn be ionized and accelerated back into the exobase resulting in a complicated feedback process (Johnson and Luhmann 1998). Since an expanded corona can push the solar wind interaction region outward, they also pointed out that this could reduce the flux of re-impacting ions, so that there may be negative feedback. Heating of thermospheres and exospheres induced by the deflected ambient plasma, pick-up ions and

re-impacting neutrals have been simulated for a number of planetary bodies, as discussed below.

4 Exospheres and Escape from Venus, Mars and Titan

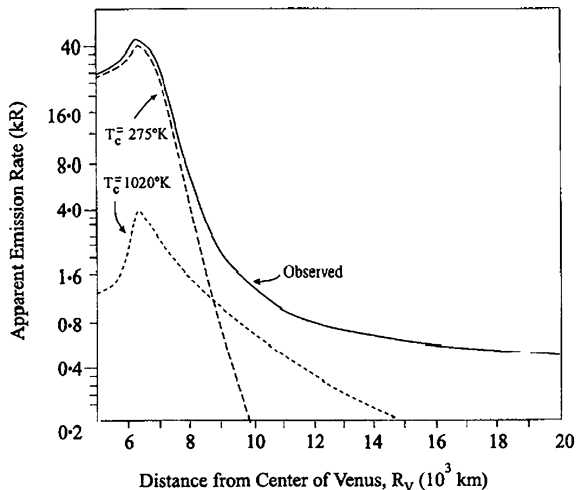
4.1 Overview

Theories of planetary exospheres have been based on ground-based and space observations of emission features such as the 121.6 nm Ly- α and 102.6 nm Ly- β hydrogen lines, the 58.4 nm helium line, and the 130.4 and 135.6 nm atomic oxygen lines. The Mariner observations indicated the presence of hot H (Fig. 3), and the Pioneer Venus UV spectrometer data established the presence of hot O and C at Venus (Nagy et al. 1981; Paxton 1985). Such observations, together with *in situ* mass-spectrometer measurements, as at Titan, allow the density and temperature height profiles of the exospheric components to be constructed. As described above, the exospheres contain hot (suprathermal) neutrals that are a manifestation of the non-thermal processes: dissociative recombination, dissociation by ultraviolet photons and electrons, and exothermic chemical reactions. These are accompanied by the release of energies on the order of several eV, part of which is stored as the internal excitation of the products (Wayne 1991). Charge exchange and atmospheric sputtering induced by energetic plasma ions also produce hot neutrals but with energies up to several hundred eV s (Johnson 1990). These hot neutral sources produce escape, determine the coronal structure, and produce nonthermal emissions. They can also affect the chemistry since non-equilibrium rate coefficients, especially for reactions with high activation energies, can be large.

4.2 Venus

The neutral and plasma environments of Venus are strongly coupled since the atmosphere is not protected by an intrinsic field (Bougher et al. 2008). Pioneer Venus Orbiter (PVO) found a robust magnetic barrier and an almost complete solar wind deflection around the exobase,

Fig. 3 H corona at Venus discovered by Mariner 5 (Anderson 1976). The emission was fit to a thermal fraction at 275 K and a non-thermal fraction at 1020 K



and the ionopause, where the solar wind and the ionospheric pressures are balanced, was located at a few 100 km altitude. The abrupt drop in ionospheric density at the ionopause is the most striking evidence that the solar wind is scavenging the upper ionosphere. Just above the ionopause is the mantle; between the mantle and the bow shock is the magnetosheath, whose properties are affected by the presence of the hot neutrals.

The exosphere alters the incoming plasma by both mass loading it with ionized gases and charge exchange producing H and O ENAs. Recent numerical estimates (Gunell et al. 2006) indicate that solar wind penetrates fairly deep into the atmosphere at solar maximum, resulting in acceleration and outflow of mainly O^+ with energies up to a several keV. On the other hand, magnetic field measurements from Venus Express (Zhang et al. 2007) show that little solar wind plasma enters the Venus ionosphere at low solar activity.

The creation of hot O is due to exothermic chemistry and to photon and electron impact, as discussed earlier, but loss to space is due mainly to sputtering. Additional loss, due to the ion escape and ionospheric outflow (Terada et al. 2004), occurs when ions produced in the corona are accelerated by the convective electric field and dragged along by solar magnetic field lines wrapping the planet.

The hot O corona at Venus is produced primarily by dissociative recombination of O_2^+ ions [(15a)–(15e)]. Simulations of the hot O have been compared with direct observations (e.g., Fig. 4a). Most simulations use hard sphere models for collisions, and heating of the atmosphere by hot atoms is not considered. Shematovich et al. (2005a), Krestyanikova and Shematovich (2006) and Shematovich and Johnson (2006) recalculated the energy distributions of hot O in thermospheres of terrestrial planets using realistic differential cross sections (e.g., Kharchenko et al. 2000). Results are shown in Fig. 4b, showing that the corona contains a significant hot O component. Using realistic scattering angle distributions resulted in a lower rate of energy loss and, consequently, a higher hot O fraction than when hard sphere models were used (Nagy and Cravens 1988; Hodges 2000). The creation and escape of a hot C corona has also been studied (Fox and Paxton 2005; Liemohn et al. 2004). They concluded that both photodissociation of CO and dissociative recombination of CO^+ and CO_2^+ are the main sources of hot C. Coupled ionosphere and thermosphere models provide important input parameters (Fox and Paxton 2005) allowing one to calculate the distribution of hot H, C, and O in the thermosphere and to estimate escape rates.

Precipitating O^+ pickup ions of exospheric origin follow helical trajectories along interplanetary magnetic field lines draped across Venus and are either swept away or re-impact the atmosphere with significant energies (up to 1 keV) causing sputtering and population of the corona. Luhmann and Kozyra (1991) suggested that 90% of the O^+ pickup ions ($\sim 1.25 \times 10^6 \text{ cm}^{-2} \text{ s}^{-1}$) re-impact producing an escape flux $\sim 2.5 \times 10^6 \text{ O cm}^{-2} \text{ s}^{-1}$. Assuming these O^+ ions impact a half sphere, the average sputter loss rate is $\sim 6 \times 10^{24} \text{ O s}^{-1}$. This is comparable with the pick-up ion loss and is the only process that produces neutral O escape at Venus.

There are two main sources for pickup: ionization of neutrals inside the corona, producing mainly of O^+ , H^+ and C^+ , and an ionospheric wind, the outflow of ions produced above the photochemical equilibrium region and below the ionopause (Terada et al. 2004). Relative escape rates depend on the composition of the ionosphere, which is determined by ion-neutral chemistry involving O_2^+ , N_2^+ , CO^+ , and NO^+ . About $10^{25} \text{ O}^+/\text{s}$ are lost through ionization of the hot oxygen exosphere in the magnetosheath and solar wind followed by magnetic drag and subsequent acceleration of the tail plasma (Luhmann et al. 2006b; Russell et al. 2006; Lammer et al. 2006). Measurements by Venus Express show that H^+ , He^+ , and O^+ are the dominant escaping ions, through the plasma sheet and in boundary

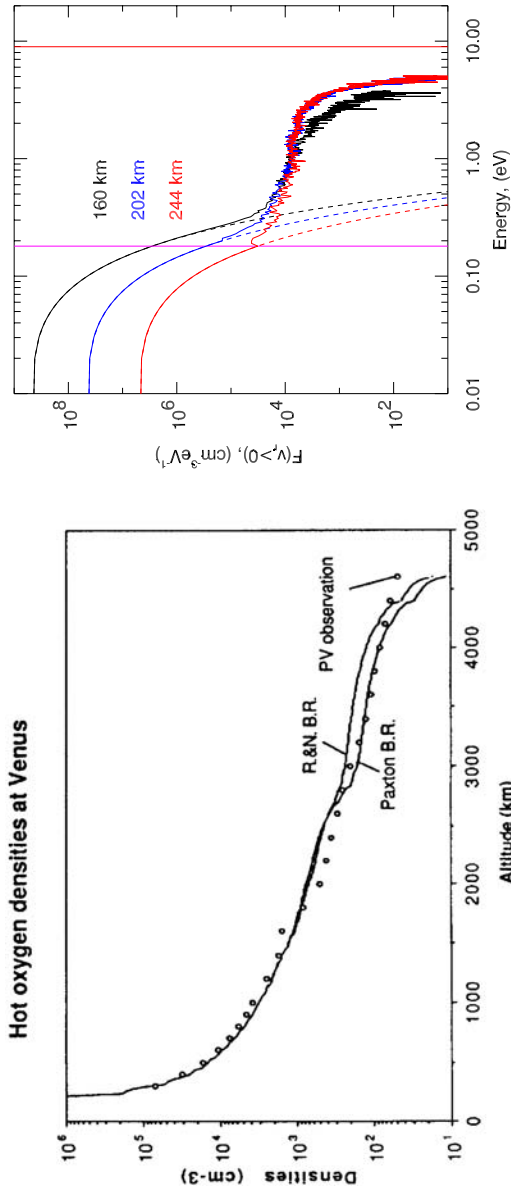


Fig. 4 (Left) Hot O at Venus. Calculated and deduced from the PVO UV spectrometer measurements for solar cycle maximum conditions (Nagy et al. 1990). (Right) Calculated kinetic energy distributions $F(v_r > 0)$ of upward moving O in Venus's upper atmosphere: solid lines: Maxwellian; dashed lines: Maxwellian; vertical line is the escape energy (~ 9 eV) (Shematovich and Johnson 2006)

layer of the induced magnetosphere, with a ratio for H^+ to O^+ of ~ 1.9 (Barabash et al. 2007b). Absolute escape rates are not yet determined.

4.3 Mars

The first measure of escape at Mars was made by Phobos 2 during solar maximum (Lundin et al. 1989). The best estimate was an ion escape rate $\sim 1\text{--}3 \times 10^{25} \text{ s}^{-1}$ of heavy ions tentatively identified as O^+ and O_2^+ (Rosenbauer et al. 1989; Lundin et al. 1989; Lundin and Dubinin 1992). However, this is very uncertain because the position and size of the plasma sheet through which the heavy ions were seen to escape and the solar conditions were not well characterized. Twenty years later, during solar minimum conditions, ASPERA 3 on Mars Express fully covered Mars' magnetotail and obtained a better estimate of ion escape: $1.6 \times 10^{23} O^+ \text{ s}^{-1}$, $1.5 \times 10^{23} O_2^+ \text{ s}^{-1}$ and $8 \times 10^{22} CO_2^+ \text{ s}^{-1}$ with an uncertainty of less than 50% (Barabash et al. 2007a). This is in agreement with 3D hybrid simulation of Mars' interaction with the solar wind (Modolo et al. 2005) as well as with 3D MHD simulations (Ma et al. 2004; Ma and Nagy 2007). It suggests either the Phobos 2 escape rates (Lundin et al. 1989; Rosenbauer et al. 1989) were significantly overestimated or the rate varies by up to two orders of magnitude from solar minimum to solar maximum.

At Venus, the global day to night motion of the ionospheric plasma is due to the horizontal pressure gradient in the subsolar region which accelerates plasma towards the nightside (Shinagawa 1996). Therefore, a global upward motion of ionospheric ions on the dayside is associated with global downward motion of ions on the nightside, a process that should occur also at Mars. Shinagawa and Cravens (1989) used a 1D multi-species magneto-hydrodynamic simulation between 100 and 480 km to model Mars' ion chemistry and ionosphere. They concluded that large scale horizontal plasma convection needs to occur in the upper atmosphere in order for their model ion profiles to fit the observations of Viking, and the solar wind appears to penetrate the upper atmosphere (Hanson et al. 1977; Johnson 1978). Fox (1997) compared her ionosphere model to Viking measurements and concluded that the main ion escaping from Mars was O_2^+ and the flux might be 4 times larger than that observed by Lundin et al. (1989) at high solar activity and around 3 times lower at low solar activity. The recent measurement by ASPERA 3 on board Mars Express indicate that the solar wind does penetrate deeply into Mars' atmosphere (Lundin and Barabash 2004) but that the tailward flux is significantly different from that in Fox (1997). This suggests the upward dayside ionospheric outflow might not be lost at Mars (Carlsson et al. 2006; Barabash et al. 2007a). In a more recent study using a global 3D multispecies MHD model, Ma and Nagy (2007) concluded that the tailward flow of ionospheric ions is a significant fraction of the ion flux measured by Lundin et al. (1989); they also successfully reproduced the Viking ion densities in a self consistent manner, without the need of ad hoc velocity assumptions.

Most of the models of Mars' interaction with the solar wind indicate that atmospheric escape is dominated by loss of neutrals (Chassefière and Leblanc 2004; Chassefière et al. 2007). To constrain escape the spatial structure, composition and size of the exosphere, and its variability with respect to solar EUV and solar wind activity need to be characterized. In fact, the presence of a hot component in Mars' exosphere is still debated. Lichtenegger et al. (2007) pointed out the discrepancy between estimates of exospheric temperature of $350 \pm 100 \text{ K}$ based on Lyman α airglow observation (Anderson and Hord 1971) and estimates of 225 K by Viking 1 and 2 probes (Nier and McElroy 1977) at low solar activity, of 220 K for moderate solar conditions by Mars Global Surveyor (Keating et al. 1998), or of $200 \pm 10 \text{ K}$ for solar minimum conditions from day-glow measurements by SPICAM/Mars

Express (Leblanc et al. 2006, 2007). This discrepancy might be explained by the presence of a significant hot H component in the exosphere like that observed at Venus (Anderson 1976; Bertaux et al. 1978). Chaufray et al. (2008) recently analyzed Mars Express observations of the Lyman α airglow and concluded that, as at Venus, a two component H exosphere fits the observed profiles: a hot component ($T > 500$ K) and a component with $T > 200$ K.

Nagy et al. (1981) and Ip (1988) were the first to describe the production of hot O by dissociative recombination of O_2^+ (15a–15e) releasing excess energies between 0.8 and 6.99 eV depending on the vibrational state of the O_2^+ , as discussed earlier. Using a two stream model (Nagy and Cravens 1988) or a test particle simulation (Ip 1988) the partial thermalization of the hot O was described by collisions with atmospheric particles. Both works noted the presence of a substantial hot O component above 500 km at solar minimum (Nagy et al. 1990; Ip 1990; Lammer and Bauer 1991). Kim et al. (1998) developed a model for the hot O exosphere taking into account the role of the vibrational state of the O_2^+ atoms, for both solar minimum and maximum with densities between 2×10^3 O/cm³ and 6×10^3 O/cm³ at 1000 km. Nagy et al. (2001) used a two stream model to conclude that photodissociation of CO is the main source of the C exosphere with densities ~ 10 – 100 C/cm³ at 1000 km (Fox and Bakalian 2001). Krestyanikova and Shematovich (2005, 2006) used a 1D DSMC simulation with accurate low energy cross-sections and found a significantly hotter O exosphere than in these models.

The sputter contribution to the exosphere (Johnson and Luhmann 1998), although negligible at low solar activity, might be of the same order as the dissociative recombination contribution for higher solar activity and even dominant in early epochs. Recently Cipriani et al. (2007) used a multi-species model of the exosphere of Mars to simulate both dissociative recombination and sputtering. They confirmed the range of densities previously predicted for hot C and O. They also concluded that the sputter contribution to the O exosphere remains significantly smaller than that due to dissociative recombination, but that sputtering populates the exosphere with CO and CO₂ molecules. The Martian hot O corona due to dissociative recombination was a factor of 10 lower at midnight than at noon (Hodges 2000) and the sputter component showed a similar variation (Leblanc and Johnson 2001). Chaufray et al. (2007) estimated the incident flux of pick-up ions incorporating the Modolo et al. (2005) 3D hybrid simulation. Accounting only for the change in the EUV activity, they concluded that at both solar minimum and maximum the contribution to the hot O exosphere by sputtering was one to two orders smaller than that due to dissociative recombination.

Extrapolation to earlier epochs (Lammer et al. 2008) remains uncertain, not only due to uncertainties in the history of the solar activity and solar wind pressure, but also because of the lack of knowledge of the dependency of the escape rate on solar conditions. Modolo et al. (2005) found a variation in the total pick-up ion loss rate by a factor 4 to 5 from solar minimum to solar maximum taking into account *only* the variation of the EUV/UV flux on the ionization rate. Ma and Nagy (2007) found a variation of a factor 2.5 in the ion escape rates due to the EUV/UV flux in going from EUV/UV minimum to maximum, whereas Harnett and Winglee (2006) found the ion loss rates between quiet solar wind conditions and fast solar wind conditions varied by a factor 1.8. Chaufray et al. (2007) examined solar minimum and maximum conditions combining an O exosphere model with the Modolo et al. (2005) hybrid model. They found a global variation of a factor 4 in the neutral escape rates and of a factor 10 in the pick-up ion flux. At Venus, Luhmann et al. (2007) correlated periods of high escape flux with high solar dynamic pressure during PVO observations. Ma and Nagy (2007) modeled this effect at Mars and found an increase in the ion escape rate of an order of magnitude at solar maximum. Therefore, it remains critical at Mars to accurately model and measure escape over a solar cycle.

4.4 Titan

Titan has a thick and extended atmosphere, which consists of over 95% N₂, about 2–3% CH₄, with H₂ and other minor species. Understanding the evolution of Titan's atmosphere provides a critical end point for understanding of the evolution of the atmospheres of the terrestrial planets (Lammer et al. 2008) and the other natural satellites (Johnson 2004). The measured D/H and ¹⁵N/¹⁴N ratios from Cassini-Huygens (Waite et al. 2005a; Niemann et al. 2005) indicate that considerable escape has occurred. The physics of the exosphere is interesting in that thermal escape (Cui et al. 2008), chemical-induced escape (De La Haye et al. 2007b), slow hydrodynamic escape (Strobel 2008b), pick-up and ionospheric ion loss (Ledvina et al. 2005; Ma et al. 2006), and atmospheric sputtering (Michael et al. 2005) have all been proposed as processes that are active at present (Johnson 2008). It is also interesting that atmospheric sputtering varies considerably depending on whether Titan is in Saturn's magnetosphere or exposed to the solar wind flux (Penz et al. 2005).

Heating effects induced by pick-up ions and energetic re-impacting neutrals have been estimated. Initial estimates for N⁺ magnetospheric ions penetrating Titan's atmosphere were large (Lammer et al. 2000). However, a DSMC model of the sputtering and heating using a model plasma flux consisting of magnetospheric and pick-up ions led to an increase of the exobase temperature of only a few K and modest loss rates (Michael and Johnson 2005). However, when Titan was within Saturn's magnetosphere, atmospheric sputtering appeared to dominate photon and electron-induced loss processes. Based on such pre-Cassini estimates, it was concluded that the present mass loss rate was small (Shematovich et al. 2003). If that was the case, processes responsible for the isotope ratios must have occurred in an earlier period when the escape processes were more robust. Following the Voyager flybys it was also assumed that ionization of the neutrals escaping from Titan would be the dominant process for supplying Saturn's magnetosphere with heavy ions (Barbosa 1987). However, such ions are rapidly lost down Saturn's magnetotail, so that the dominant source of nitrogen ions to Saturn's magnetosphere is Enceladus (Smith et al. 2007; Johnson et al. 2008). In spite of this, Titan remains an important source of mass loading and plasma in the outer magnetosphere.

With the many transits of Titan's exobase by Cassini, the escape processes can now be characterized. At this writing, data from the Cassini ion neutral mass spectrometer (INMS) have been used to obtain new escape rates. De La Haye et al. (2007a, 2007b) examined the INMS data for a number of early passes and showed that the energy spectra of the molecules in the corona have, not surprisingly, a hot component. In order to simulate the densities of N₂ and CH₄ in a region extending ~ 500 km above the exobase, the molecular energy spectrum was best represented by a kappa distribution. More importantly, for four of the five exobase crossings examined, they could not account for the observed corona structure by assuming that the hot component was only populated by photon and electron induced processes, and concluded that plasma-induced heating associated with the magnetosphere ionosphere interaction must be important. Assuming that is the case, then scaling the required energy deposition rate to a model plasma flux (Michael et al. 2005), a net escape flux is obtained of ~ 0.3–1 × 10¹⁰ amu/cm²/s measured with respect to Titan's surface (De La Haye et al. 2007a). Using the analytic recoil distribution for the hot component gave a rough upper bound of about 5 × 10¹⁰ amu/cm²/s normalized with respect to Titan's surface. More recently Cui et al. (2008) found an H₂ escape rate ~ 10¹⁰ amu/cm²/s. In addition a globally average value of ~ 5 × 10¹⁰ amu/cm²/s (4.5 × 10²⁸ amu/s divided by 4πR_T²) was estimated by assuming slow hydrodynamic escape, as described in Sect. 3.1.2 (Strobel 2008a). Finally,

modeling diffusion separation and flow, Yelle et al. (2008) inferred $\sim 4\text{--}5 \times 10^{10}$ amu/cm²/s for CH₄ loss. Remarkably, such rates are equivalent to losing a mass equivalent to the present atmosphere in ~ 4 Gyr. Therefore, loss rates may be much larger than pre-Cassini predictions, but this large loss rate and the mechanism are not agreed upon Johnson (2008). Since plasma-induced heating in the exobase region appears to be a major source of energy, understanding the plasma flow through the transition region is critical for describing the escape rates and structure of the thermosphere and the corona.

5 Exospheres and Escape from Small Bodies

5.1 Io Atmosphere and Torus

The Galilean satellites of Jupiter are instructive for studies of the escape processes in Sect. 3. The most extensively studied is Io, where the first indications of its tenuous atmosphere were the detection of an ionosphere by the Pioneer 10 radio occultation and detection of escaping Na by Brown (1974). SO₂ was subsequently detected by the Voyager IRIS (Pearl et al. 1979) and has been observed since 1990. It was initially unclear whether Io's atmosphere was global or confined to the dayside, where the sublimation of SO₂ frost is orders of magnitude higher than on the night side, and whether the exobase is at or above the surface (McGrath and Johnson 1987). The atmosphere is now understood to be global, although highly non-uniform, and the exobase is variable and above the surface across most of the satellite.

Global characterization of the atmosphere was made by imaging Io using the HST Imaging Spectrograph at the Lyman- α wavelength (1215.67 Å) where SO₂ absorbs strongly, decreasing the surface reflectivity where it is densest. The dayside map in Fig. 5 shows SO₂ is densest at the equator and on the anti-Jovian hemisphere. The sources are active volcanism, sublimation, and, to a lesser degree, sputtering by the Jovian magnetospheric ions that penetrate the atmosphere and reach the surface. Dissociation products, S, O₂, and SO are present at lower abundances, as are minor species (Na, K, Cl, NaCl) which, along with S₂, originate in active volcanoes.

The largest volcanic plumes, such as Pele and Tvashtar, can attain heights of several hundred kilometers. Nonetheless, the best models indicate that plume gas velocities are

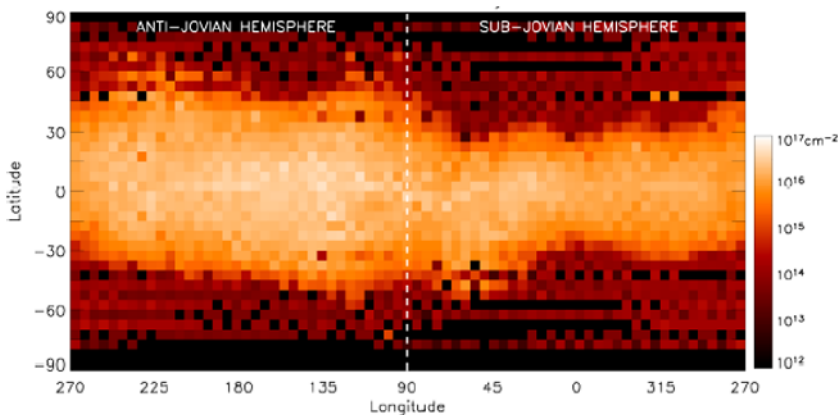


Fig. 5 Map of the SO₂ column density for Io's dayside atmosphere (Feaga et al. 2007)

well below the escape velocity. Therefore, volcanic gas does not escape directly, but contributes to the atmosphere and condenses on the surface. The characteristics of Io's night-side atmosphere are essentially not measured, but active volcanoes will maintain an SO₂ component. The pressure varies significantly from day to night, driving winds that transport the volatile dissociation products, O₂ and, possibly, SO, to the night side (Wong and Johnson 1996; Smyth and Wong 2004). Adding to the complexity is the fact that the magnetospheric plasma continually bombards the atmosphere providing an additional heat source, sputtering. The complicated environment and the spatial and temporal variability of the sources make development of self-consistent models challenging. Nevertheless, it is generally agreed that the exobase altitude varies considerably across the surface and molecular species are present at the exobase.

The interaction between Io's atmosphere and Jupiter's magnetospheric plasma results in mass loss of about one ton per second. As with the other bodies discussed, some of this material is lost from Io in the form of ions, while the principal fraction escapes as neutrals. These neutrals attain enough energy to escape from Io, but, for the most part, not from Jupiter. Therefore, they orbit Jupiter forming large neutral clouds whose morphology reflects the ejection and loss mechanisms. Ejected neutrals are eventually ionized, primarily by electron impact or charge exchange. They are then picked-up and accelerated to the velocity of the rotating magnetic field and swept into a plasma torus surrounding Jupiter at the orbital distance of Io. The plasma torus settles at the centrifugal equator, which is tilted $\sim 7^\circ$ with respect to Io's orbital plane, while Jupiter's magnetic field is tilted by 10° with respect to this plane. The plasma overtakes Io and continually re-impacts the atmosphere ejecting neutrals while the accompanying fields pick-up and remove newly formed ions.

The plasma-induced escape processes have been traced by atomic sodium observations. Although its density is low, Na efficiently fluoresces, with an emission intensity 30 times brighter than any other species at visible and near infrared wavelengths. Therefore, it has been readily observed both near and far from Io since the early 1980s (McGrath et al. 2004). Escape processes for sulfur and oxygen species are less visible, but are modeled by analogy with sodium. Fig. 6 shows images of Na emission at several different scales, illustrating the operative escape mechanisms. The "jet" and "stream" features in the left panel are associated with fast escape, while the "banana" feature is associated with slow escape. The directionality of these features relative to the background magnetic field provides the key to their origins.

Fast Na atoms, associated with the jet and stream features, are a result of Io being immersed in the Jovian magnetic field and plasma. The inclination of the plasma torus relative to Io's orbital plane means that in the course of a ~ 10 hr Jupiter rotation, Io encounters the densest region of the plasma torus twice. The Na jet is a narrow feature that extends away from Io in the anti-Jupiter direction. Its orientation oscillates over a period of several hours correlated with Io's magnetic longitude (Pilcher et al. 1984). It points approximately perpendicular to the local unperturbed magnetic field at Io (Wilson and Schneider 1999). This directionality indicates that the motional electric field drags ions out of the top of Io's anti-Jovian ionosphere, which eventually produce fast neutrals.

The Na stream is a long, narrow feature leading Io in its orbit; it undulates above and below the plasma torus equator with the same period as the jet. The difference between the stream and the jet is the timescale for neutralization of the fresh, approximately corotating, pickup ions. The ions which form the stream recombine in the torus a few hours after leaving Io, whereas those in the jet take only minutes or less to recombine close to Io. In order to produce the observations, the Na in the stream must be produced in ≤ 10 hours. This is incompatible with Na⁺ recombination, so the stream must be formed by recombination of

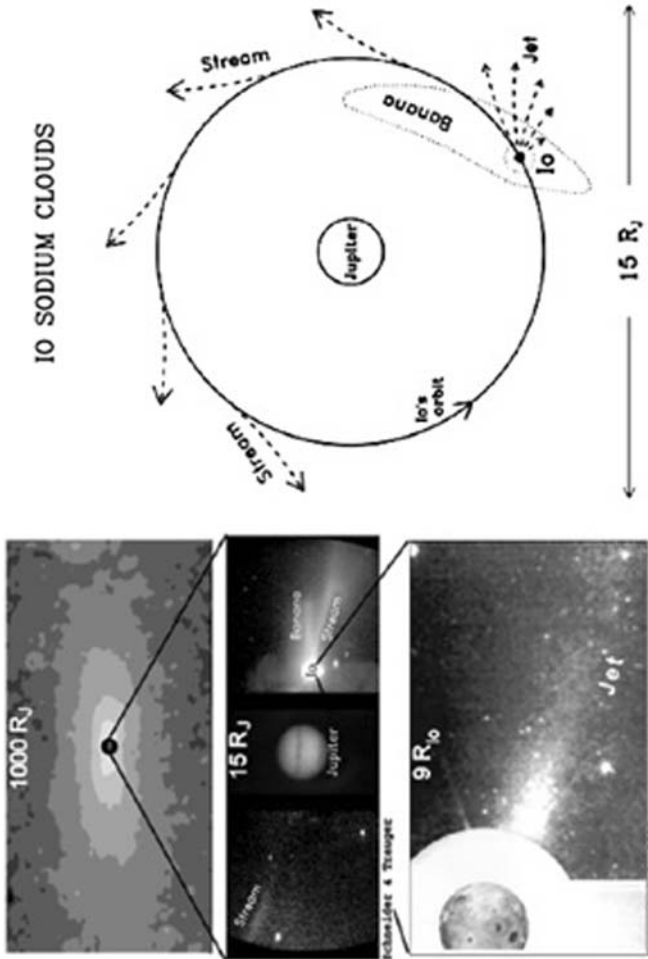


Fig. 6 *Left:* Images at three different scales illustrating the Na escape processes at Io. The width of each image is given by the number at the *top* ($1R_J = 7.14 \times 10^4$ km). *Top:* Na emission from a cloud that is visible to distances of $500R_J$ (Mendillo et al. 1990). *Middle:* Image encompassing Io's orbit showing the Na stream feature (Schneider and Trauger 1995). *Bottom:* The Na jet in the near-Io environment (Burger et al. 1999). The diagram at *right* illustrates the different features schematically (Thomas et al. 2004)

NaX^+ from the ionosphere (Schneider et al. 1991). It is possible that the jet is also produced by escaping NaX^+ ions. The jet may simply represent higher dissociative recombination rates in the part of the stream closest to Io where plasma densities are greatest. The parent, NaX^+ , has not been identified, but molecular ions of S and O are obvious candidates (Johnson 1994).

Specific reactions at work in producing the fast features are: charge exchange ($\text{Na}_{\text{iono}}^+ + \text{Na}_{\text{atmo}} \rightarrow \text{Na}_{\text{fast}} + \text{Na}^+$); dissociative recombination ($\text{NaX}_{\text{iono}}^+ + e^- \rightarrow \text{Na}_{\text{fast}} + \text{X}_{\text{fast}}$); impact dissociation ($\text{NaX}_{\text{iono}}^+ + e^- \rightarrow \text{Na}_{\text{fast}} + \text{X}^+ + e^-$). It is uncertain to what extent similar S and O streams and jets exist. Photochemical equilibrium in a collisionally thick and static ionosphere would be dominated by Na^+ and K^+ because of their relatively low ionization potentials (Kumar 1985; Moses et al. 2002), suggesting that if the jet is produced by escaping atomic ions, it may be unique to Na and K. However, the atmosphere is not static and in-situ measurements by the Galileo spacecraft detected signatures near Io at frequencies close to the gyrofrequencies of SO_2^+ and SO^+ (Kivelson et al. 1996; Warnecke et al. 1997), implying that streams or jets of S and O are probably present. The Cassini spacecraft found evidence of extended clouds of S, O, and SO_2 escaping from the Jupiter system via detection of fresh pickup ions (including SO_2^+) well upstream of Jupiter (Krimigis et al. 2002). The parent neutrals most likely result from charge exchange of S^+ , O^+ and SO_2^+ with the neutrals in the Io torus, a process which is less important for sodium.

The so-called Na “banana feature” in Fig. 6 is produced by atmospheric sputtering induced by plasma torus or escaping ionospheric ions. Many of the hot neutrals produced do not escape but heat and expand Io’s atmosphere (Pospieszalska and Johnson 1996; McGrath et al. 2004). Elastic collisions primarily generate low-energy recoils so that most ejected neutrals have speeds of about a few km/s. These form large clouds extending both ahead of and behind Io, approximately along its orbit. Neutral clouds of sulfur (Durrance et al. 1983, 1995), oxygen (Brown 1981; Durrance et al. 1983; Thomas 1996), and potassium (Trafton 1981) have been detected in addition to Na. These clouds are confined close to the orbital equator, while the plasma torus is confined to the centrifugal equator. The clouds intersect the densest regions of the torus every 6.5 hours, where they are subject to elastic collisions, electron impact dissociation, and ionization, which limit their extent both ahead of and behind the satellite. The complex interplay of ejection speed and direction, orbital motion, and ionization lifetime gives the Na cloud its banana-like shape.

Oxygen and sulfur, due to their higher abundances in Io’s atmosphere and proportionally higher sputtering rates, combined with their different ionization lifetimes, will have different morphologies as modeled for O by Smyth and Marconi (2000). The lifetimes against electron impact ionization for sodium, potassium and sulfur are relatively short (2–5 hours) in the densest regions of the torus. The rate coefficient for O, however, is at least an order of magnitude smaller than for S so that charge-exchange loss with torus ions is dominant. The minimum lifetime for O is around 20 hours (Thomas 1992) resulting in significant neutral densities remote from Io and a much more extended, nearly toroidal cloud. Around 180° away from Io itself, densities of neutral O and S are $\sim 29 \pm 16 \text{ cm}^{-3}$ and $6 \pm 3 \text{ cm}^{-3}$ respectively (Skinner and Durrance 1986). Lagg et al. (1998) derived an average density of 35 oxygen atoms cm^{-3} using measurements from the Galileo energetic particle detector.

5.2 Icy Galilean Satellites

Much less is known about the atmospheres/exospheres and escape for Europa, Ganymede and Callisto (see recent review: Johnson et al. 2008). Molecular oxygen, predicted to be the dominant component and produced by the plasma-induced decomposition of the surface ice

(Johnson et al. 1982; Johnson 1990), was confirmed to be present at Europa and Ganymede from the ratio of atomic oxygen emission lines by Hall et al. (1995, 1998). The derived column abundances (a few $\times 10^{14}$ cm $^{-2}$ disk average value) was close to the predicted value at Europa (Johnson et al. 1982) and indicates that the exobase is at or near the surface for both satellites. Laboratory data showed that O $_2$ and H $_2$ are directly produced and ejected from water ice by the incident plasma (Brown et al. 1982; Johnson et al. 2003), a process called radiolysis. Because H $_2$ escapes more readily, forming a neutral torus (Shematovich et al. 2005b; Smyth and Marconi 2006), and the O $_2$ does not stick efficiently or escape efficiently, the atmosphere is dominated by O $_2$, even though the sputtered flux of H $_2$ O dominates. Both Europa and Ganymede also possess ionospheres, detected by Galileo radio occultations (Kliore et al. 1997), which also provided estimates of the neutral column densities.

However, follow up observations of Europa with HST (McGrath et al. 2004, 2008) showed a complex morphology for the O emission, inconsistent with the picture of a uniformly distributed exosphere. Saur et al. (1998) assumed a model O $_2$ atmosphere which differed significantly from those produced in simulation (e.g., Shematovich et al. 2005b) but described the plasma interaction and production of the O $_2$. They were able to reproduce the disk averaged HST-GHRS intensities and the nearly uniform O limb UV emission, but not the bright spot emission morphology observed with HST-STIS (cf. McGrath et al. 2004), which may be due to nonuniform sources, nonuniform surface reactivity, or nonuniform plasma excitation (Cassidy et al. 2007). Cassini Observations (Hansen et al. 2005) showed that the OI 1304 emission is more extended than the OI 1356 emission at Europa, which they interpreted as the oxygen exosphere being more extended than the O $_2$ component consistent with simulations (Shematovich et al. 2005b). Both follow up HST observations and the Cassini observations show emissions from Europa vary significantly in time.

Na and K have both been detected far from Europa (Brown and Hill 1996; Brown 2001; Leblanc et al. 2005). The sodium is also produced by surface sputtering with $\sim 40\%$ of the ejected Na having sufficient energy to escape and with the returning Na redistributed across Europa's surface (Johnson 2000; Leblanc et al. 2002b). The sputtered sodium is ionized primarily by electron impact; photoionization and charge exchange with Io plasma torus ions are negligible (Burger and Johnson 2004; Smyth and Combi 1997). The lifetime is a function of distance from Jupiter, distance from the centrifugal equator, magnetic longitude and local time and varies between 18 and 34 hours at Europa's orbit. Europa's sodium cloud is predominantly a trailing cloud, opposite to the sodium cloud at Io (Burger and Johnson 2004). Mauk et al. (2003) detected energetic neutrals, resulting from charge exchange between protons and the Europa neutral cloud, most likely due to H and H $_2$ produced by radiolysis and escape (Shematovich et al. 2005b; Smyth and Marconi 2006). Lagg et al. (2003) also reported the depletion of protons with pitch angle of 90°, which are consistent with the presence of an equatorially confined cloud of neutral hydrogen near Europa.

Only a handful of observations exist for the atmospheres of Ganymede and Callisto (Hall et al. 1998; Feldman et al. 2000; Carlson 1999), none of which includes escaping neutrals. Like Europa, Ganymede's atmosphere is dominated by molecular oxygen, but its excitation and morphology are very different because of Ganymede's internal magnetic field. The UV oxygen emissions do not exhibit the features of a globally distributed exosphere. Instead they exhibit a morphology more analogous to auroral emissions on Earth caused by the precipitation of plasma in Ganymede's polar regions. Visible emissions are confined to the equatorial regions, inconsistent with the UV emissions. Neither Na or K have been detected at Ganymede.

The component of Callisto's atmosphere that has been detected is CO $_2$ (Carlson 1999). A denser molecular oxygen component has been inferred from the ionosphere detections

(Kliore et al. 1997), but attempts to detect O₂, if present, via UV emissions have been unsuccessful (Strobel 2002). However, these observations set an upper limit for CO.

5.3 Saturn Satellite and Ring Atmospheres and Tori

5.3.1 Saturn's Ring Atmosphere

Due to its large area the Saturnian ring system should have an extended gaseous envelope, produced by micrometeoroid impact, photosputtering or energetic ion sputtering. However, because the main rings efficiently absorb energetic particles, the energetic ion flux from the magnetosphere is negligible and is dominated by a low flux of very energetic ions produced by cosmic ray impacts (i.e., the CRAND process; Cooper 1983). Using the interplanetary meteoroid flux of $3 \times 10^{-17} \text{ g cm}^{-2} \text{ s}^{-1}$ (Cook and Franklin 1970), Haff et al. (1983) estimated that the water vapor production rate from micrometeoroid-impacts could be $\sim 5 \times 10^6 \text{ H}_2\text{O}/(\text{cm}^2 \text{ s})$ ($\sim 10^{27} \text{ H}_2\text{O s}^{-1}$ averaged over the ring system; see also Ip 1984a; Pospieszalska and Johnson 1991). The emitted H₂O molecules, however, re-condense on ring particles, which have temperatures $\sim 80\text{--}100 \text{ K}$, resulting in an average column density that is small ($\sim 10^{11}/\text{cm}^2$). Therefore, Ip (1995) suggested that the O₂, which does not re-condense at these temperatures, is created from the photodissociative products (O and OH) and might have a long lifetime in the ring system leading to the formation of a tenuous, but possibly detectable, atmosphere with average density $\sim 3 \times 10^3 \text{ O}_2/\text{cm}^3$. However, as at Europa, O₂ is also directly produced by charged particle and photo-induced decomposition of ice (Johnson and Quickenden 1997; Johnson et al. 2003). Using laboratory experiments in which ice is exposed to a Lyman-alpha photo-flux (Westley et al. 1995), O₂ was estimated to be produced at a rate $\gtrsim 10^6 \text{ cm}^{-2} \text{ s}^{-1}$ by the solar EUV/UV flux (Johnson et al. 2006). The interplanetary meteoroid flux at the rings is still very uncertain. If a rate as high as $5 \times 10^{-14} \text{ g cm}^{-2} \text{ s}^{-1}$, given by Cuzzi et al. (2002) is used, the water vapor production from the ring place would be on the order of $3 \times 10^9 \text{ H}_2\text{O cm}^{-2} \text{ s}^{-1}$ ($\sim 5 \times 10^{29} \text{ H}_2\text{O/s}$ averaged over the ring system) thus making meteoroid impact a significant contributor to a ring atmosphere (Ip 2005).

During the Saturn Orbital Insertion (SOI) on July 1, 2004, the Cassini spacecraft flew over the ring plane permitting in-situ observations by the plasma instruments. The INMS (Ion Neutral Mass Spectrometer) and the CAPS (Cassini Plasma Spectrometer) experiments detected the presence of O⁺ and O₂⁺ ions (Tokar et al. 2005; Waite et al. 2005b). A flux of thermal electrons ($\sim 0.6\text{--}100 \text{ eV}$) was also detected and found to be in anti-correlation with the optical depth of the rings (Coates et al. 2005), but the neutral atmosphere was below the INMS detection threshold ($\sim 10^5 \text{ cm}^{-3}$). These results triggered an avalanche of theoretical studies on the formation and structure of the ring atmosphere (Johnson et al. 2006; Bouhram et al. 2006; Luhmann et al. 2006a; Ip 2005). Figure 7 summarizes such simulations showing the spatial distributions of O₂, O₂⁺, and O⁺ above and below the ring plane.

During SOI the solar zenith angle was about 66° below the ring plane. Therefore, only the southern side of the ring system was exposed to the solar flux emitting O₂. The ejected O₂ do not condense out, but thermally equilibrate with the ring particle surfaces. Therefore, equilibrated O₂ exists above and below the ring plane with a scale height $\sim 0.013 R_S$ (780 km). The net column density is determined by the destruction rate due to photo-dissociation and ionization.

The O₂⁺ and O⁺ ions formed by photoionization will be picked-up and accelerated by the Saturn convective electric field and characterized by their gyromotion giving flat pitch angle distributions. Given the small northward shift ($\sim 0.04 R_S$) of the magnetic dipole center,

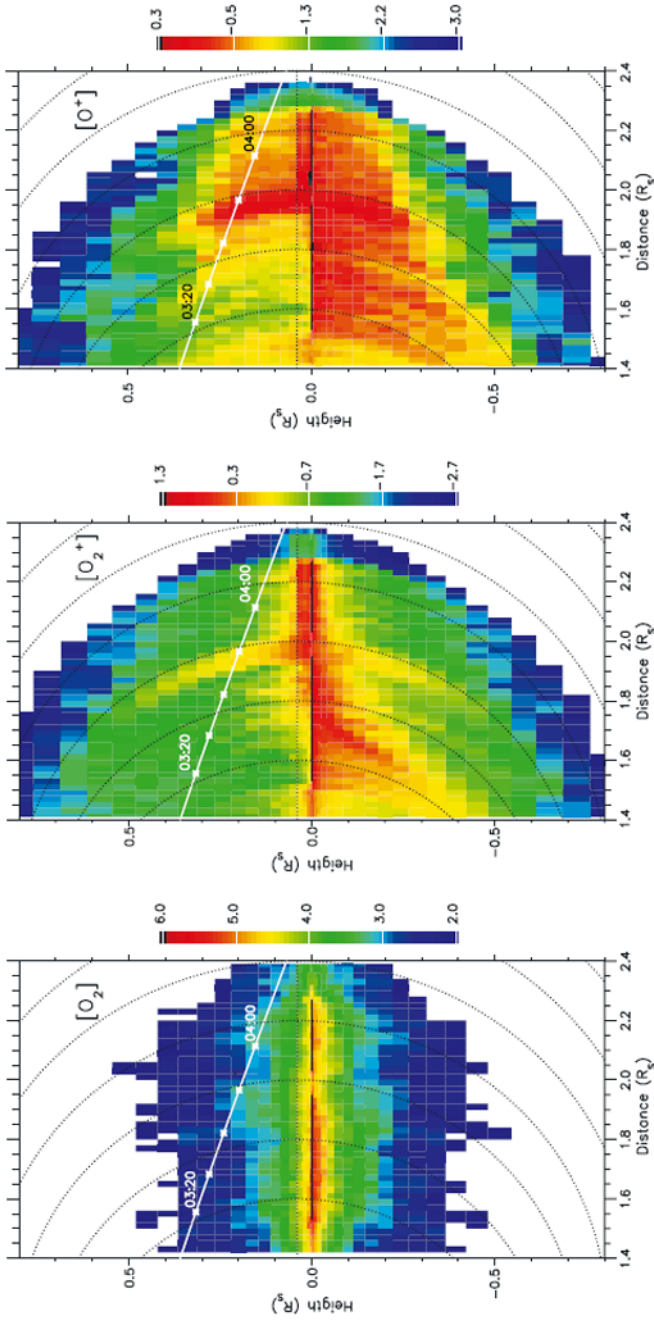


Fig. 7 Density maps from a test-particle simulation of O_2 molecules, O_2^+ and O^+ ions in the vicinity of the Saturnian rings: *white line* is the Cassini trajectory (Bouhrām et al. 2006)

O_2^+ ions will be formed in a disc-like region below the magnetic equator. The speed of co-rotation becomes smaller than the neutral orbit speed within $\sim 1.86R_S$, therefore pick-up ions formed at smaller distances from Saturn can be pulled into the southern hemisphere of Saturn (Luhmann et al. 2006a; see also Northrop and Hill 1983; Ip 1983a, 1984b) as suggested by the 2nd and 3rd panels in Fig. 7. Therefore, a steep drop in the ring-ion density was seen by CAPS at $\sim 1.86R_S$. This pickup ion motion instability limit is almost the same as the sharp boundary between the B ring and the C ring, thus the erosion of the rings might be closely related to the production of the ring atmosphere and the injection of oxygen species ions into the Saturn atmosphere at low latitudes (Connerney and Waite 1984; Moses and Bass 2000; Moses et al. 2000; Moore et al. 2006; Moore and Mendillo 2007).

The O^+ and O_2^+ are subject to ring absorption as they move along the magnetic field lines threading through the ring plane. This loss is indicated by the depletion of the ion densities above the ring plane in Fig. 7. Electrostatic charging of the ring particles can also modify the spatial distribution of these ions (Ip 1984b). The presence of a small electrostatic potential (Φ) can determine whether these low energy ions will be repelled ($\Phi > 0$) or absorbed ($\Phi < 0$) by ring particles. Due to the diurnal variations of the Saturnian ionosphere and the ring shadow, plus the corresponding seasonal changes of the incidence angle of the solar photons on the ring plane, the coupling between the ring atmosphere and the ring plasma system can be highly complex. Farmer and Goldreich (2007) examined the collisional interaction between the neutral ring gas and the ion component to see if there is a strong electrodynamic effect, as suggested by the ring spoke phenomenon (Goertz and Morfill 1983; Farmer and Goldreich 2005; Morfill and Thomas 2005). These authors derived an upper limit of $N < 2 \times 10^{15} \text{ cm}^{-2}$ for the column density of the oxygen molecules consistent with the models (Johnson et al. 2006).

The Cassini spacecraft flew well above the magnetic equator, therefore the detected ions came from a population that had a significant pitch angle distribution. Whereas the O^+ are formed from O_2 with an additional, randomly oriented, kinetic energy, as discussed earlier, the O_2^+ is formed with no additional kinetic energy. Therefore, the O_2^+ detected at altitudes $\gtrsim 0.1R_S$ were scattered by charge exchange collisions with O_2 molecules (Johnson et al. 2006). This process also injects O_2 into the Saturnian magnetosphere contributing to O_2^+ detected outside of the ring system (Tokar et al. 2005; Young et al. 2005; Krimigis et al. 2005). Therefore, the aeronomy occurring in Saturn's tenuous ring atmosphere could be the key to the understanding of an array of fundamental issues in the Saturnian system ranging from the large-scale structure of the ring system, the spoke phenomenon, the aeronomy of the Saturnian atmosphere, and the magnetospheric composition and dynamics.

5.3.2 Enceladus and the E-ring

HST observations (Shemansky et al. 1992) showed that the Saturnian system is immersed in a cloud of H_2O and its dissociation products that is much more robust than initially predicted (Johnson et al. 1989). The OH density was estimated to be $\sim 160 \text{ cm}^{-3}$ at $L \sim 4.5R_S$, but subsequent HST observations (Hall et al. 1996; Jurac et al. 2002) showed this density could be as much as $\sim 1000 \text{ cm}^{-3}$ at this radial distance. The detected OH cloud is the product of dissociation of H_2O molecules ejected from the icy bodies that orbit at such distances from Saturn. Therefore, the key question became how to account for the source of the circum-planetary water cloud. After a long series of modeling efforts (Johnson et al. 1989; Pospieszalska and Johnson 1991; Richardson 1998; Ip 1997, 2000), Jurac et al. (2002) showed that the principal source region was near the orbit of Enceladus with a strength of $\sim 0.4 \times 10^{28} \text{ H}_2\text{O/s}$. Treating the plasma and neutrals self-consistently, Jurac and Richardson

(2005) confirmed the source region, but increased the rate to $\sim 10^{28}$ H₂O/s. Such source rates could not be due to sputtering or meteoroid impact processes, but to some more robust process occurring near Enceladus' orbital radius.

On its way in towards the Saturn system, the Ultraviolet Imaging Spectrometer (UVIS) experiment on the Cassini spacecraft found high temporal variability in O emission over an extended region as seen in Fig. 8a (Esposito et al. 2005). The emission represented a minimum production and loss of $\sim 4 \times 10^{34}$ O over a time interval of three months (an average $\sim 0.5 \times 10^{28}$ /s). Although Haff et al. (1983) conjectured that the E-ring grains, which co-orbit with the neutrals seen by HST, might be emitted from geysers on Enceladus, not much attention was paid to this suggestion since no adequate heat source could maintain a subsurface liquid reservoir on this small satellite (Squyres et al. 1983). The situation has now completely changed because of the surprising discovery by the Cassini spacecraft of outgassing at the south pole of Enceladus often referred to as geysers or jets, Fig. 8b.

The magnetometer on Cassini detected perturbations in Saturn's field which suggested that ion formation was occurring close to Enceladus (Dougherty et al. 2006). On July 14, 2005, the spacecraft flew by Enceladus at a closest approach distance of 175 km from its surface. A system of linear fractures (called "Tiger Stripes") was observed by Cassini at the south pole of Enceladus (Porco et al. 2006). In addition, the infrared instrument (CIRS) showed that the temperature was anomalously high indicating the existence of an interior heat source (Spencer et al. 2006). The ISS experiment and the Cassini Dust Analyzer (CDA) also detected the existence of a system of dust jets emanating from the south pole (Fig. 8b), with the "Tiger Stripes" the most likely source. The INMS experiment (Waite et al. 2006) measured an extended distribution of gas cloud composed of H₂O (91%), CO₂ (3.2%), CO or N₂ (3.3%) and CH₄ (1.7%). The radial density distribution of the water molecules suggested the plume could be characterized by two components, one that decayed as $\sim r^{-2}$ from the south polar region plus a minor component, which varied more steeply and appeared to be emitted uniformly over the surface. From the UVIS observation of the occultation of lambda Scorpii by the Enceladus plumes, Hansen et al. (2006) found the production rate that was consistent with that predicted by Jurac and co-workers (Jurac et al. 2002; Jurac and Richardson 2005). Monte Carlo modeling of the ejecta were carried out, assuming a speed distribution and a source rate consistent with rapid sublimation at ~ 180 K (i.e., a thermal surface flux with an energy distribution $[E \exp(-E/kT)/(kT)^2]$ and a cosine distribution corresponding to mean flow speed at the surface of 0.36 km/s on a body with an escape speed 0.24 km/s). The ejecta produced a narrow neutral torus ($\lesssim 0.5R_S$), and the much larger OH torus, seen earlier by HST, was produced by charge exchange scattering of neutrals from the narrow Enceladus torus (Johnson et al. 2006). In a three-dimensional Monte Carlo model, Burger et al. (2007) showed that the local neutral distribution close to Enceladus could be accounted for by a global source $\sim 8 \times 10^{25}$ H₂O s⁻¹ and a localized source at the south pole $\sim 10^{28}$ H₂O s⁻¹. Modeling of the formation and flow of plasma in Enceladus' escaping atmosphere is underway and has much in common with modeling of comet atmospheres discussed below.

5.4 Triton and Pluto

Pluto and Triton, a satellite of Neptune, are twin Kuiper-belt objects. Both have N₂ dominated atmospheres with Pluto having significantly more CH₄. Methane absorbs near-IR solar radiation generating a quasi-isothermal, ~ 100 K, stratosphere that is hotter than Triton's but both have thermospheres with $T \sim 100$ K. In the absence of data for escape from Pluto, models favor a hydrodynamically escaping atmosphere, as described earlier, with limiting diffusive fluxes for CH₄, H₂, H and total mass loss rates limited by the net heating rate.

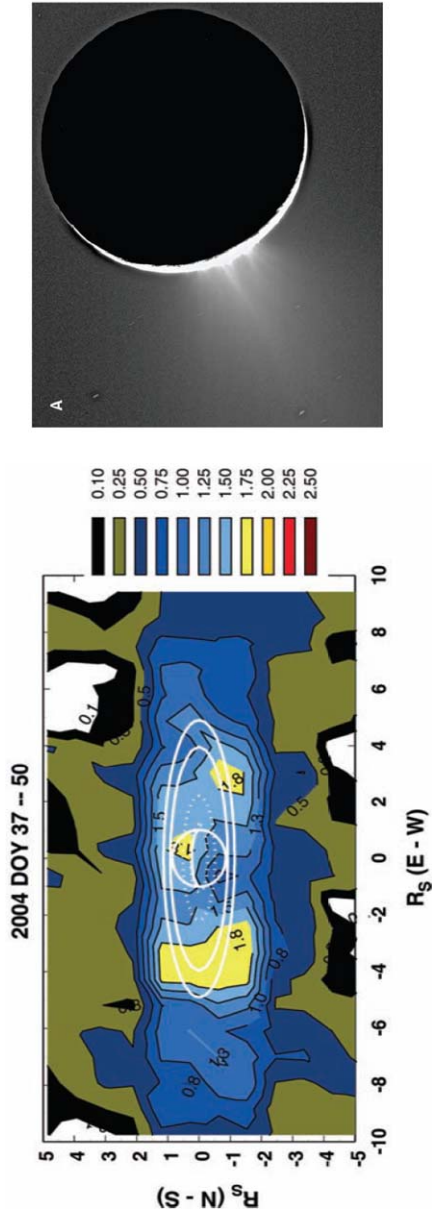


Fig. 8 (a) O emission from the Saturn system obtained by Cassini UVIS experiment from $\sim 1000R_S$ (Esposito et al. 2005); (b) ISS NAC clear-filter image of Enceladus' near-surface plumes taken on 27 November 2005 at a phase angle of 161.4° (Porco et al. 2006)

The actual N₂ escape rate is not settled. Tian and Toon (2005) obtained $\sim 1.5 \times 10^{28}$ N₂/s for solar minimum at 30 AU, which is an order of magnitude larger than the estimate by Krasnopolsky (1999), even though they had a factor of 5 lower heating rate due to neglect of CH₄ heating. Strobel (2008b), using a similar model, found a rate in essential agreement with Krasnopolsky (1999), but $\sim 20\%$ larger. The limiting CH₄ escape rate is proportional to its mixing ratio: e.g., for 3%, CH₄, the loss rate would be $\sim 2 \times 10^{27}$ s⁻¹. The calculated N₂ loss rates are power limited and, hence, so are mass escape rates, which include CH₄, H₂, etc. Thus higher CH₄, H₂, etc., mixing ratios and escape rates imply lower N₂ escape rates. The encounter with New Horizon spacecraft will occur in 2015 to study the atmospheric loss rates and the surface-atmosphere interactions.

Voyager 2 solar occultation measurements for Triton's upper atmosphere were used to evaluate the Jeans escape rate. Nitrogen atom densities were extrapolated from 550 km to the 930 km N₂ exobase. Escape rates for H, H₂, C, and O are based on photochemical calculations assuming Jeans escape. The values of λ at the exobase for H, H₂, N, and N₂ are 0.75, 1.5, 10, and 21, respectively. Calculated rates for total H atom (H + 2H₂) and N atoms are $\sim (7-9) \times 10^{25}$ and $(6-7) \times 10^{24}$ s⁻¹ (Strobel et al. 1995; Kotova et al. 1995). The latter also estimated rates for C and O: $\sim 1.1 \times 10^{24}$ and 4.4×10^{22} s⁻¹. For Pluto, λ values for H, H₂, N, and N₂ are 0.27, 0.54, 3.8, and 7.6 at the N₂ exobase, about a factor of 3 lower than at Triton. However, given the recent evidence for a nearly limiting CH₄ escape flux on Titan, where $\lambda \sim 25$ at the exobase, the possibility of slow hydrodynamic expansion at Triton, which has intermediate values of λ , needs to be examined.

5.5 Comets

The astronomical feature called a coma is the escaping exosphere of a small primitive icy/rocky body (Combi et al. 2004). The exosphere orbits the sun along with the body (the nucleus) and is composed of a head of gas and dust (the coma) and is often accompanied by dust and plasma tails. Beginning with the work of Whipple nearly 60 years ago, we know that the coma and tail of a comet, which can extend from thousands to millions of kilometers in size, are produced by solar heating of a relatively small dark nucleus a few kilometers across. The study of their composition is important because comets are thought to be the least processed remnants from the formation of the solar system. Observations of the coma and tail are important even today in the age of comet missions. While critical information is gained from in situ spacecraft measurements, only a handful of comets have been or will be studied directly even into the next several decades. On the other hand, the compositions of the coma and tail of hundreds of objects are observed remotely and can place the spacecraft measurements in context. Except when comets are observed far from the sun, their nuclei are always shrouded by the coma. Therefore, gaining an understanding of the structure and composition of cometary comae (or exospheres) remains an important task

The nucleus is composed of frozen volatiles that are seen in the coma, as well as the organics and refractory materials that are released in the form of small dust particles during sublimation. Given that gravity is negligible, all but the centimeter sized or larger particles are lifted by the drag force of the expanding gas. As the density of the expanding gas decreases, the dust particles continue to move outward. The ejected molecules and dust follow ballistic orbits under the influence of solar gravity and solar radiation pressure forming the dust tail and the coma. Eventually the parent molecules are dissociated and ionized producing a suite of radicals, atoms and ions. The ions interact with the magnetized solar wind and are dragged into a tail that is often seen via the fluorescence emissions of, mostly, CO⁺ and H₂O⁺ ions.

Table 1

Comet	S (s^{-1})	R_{coll} (km)
1995 O1 Hale-Bopp (1 AU)	1×10^{31}	240,000
1P/Halley (0.9 AU)	7×10^{29}	16,700
1996 B2 Hyakutake (1 AU)	2×10^{29}	4800
19P/Borrelly-81P/Wild2-9P/Tempel 1 (perihelion)	2×10^{28}	480
67P/Churyumov-Gerasimenko (perihelion)	1×10^{28}	240
67P/Churyumov-Gerasimenko (3 AU)	6×10^{25}	surface

The main scientific goal of the Deep Impact mission was to hit the nucleus of comet 9P/Tempel 1 with a high speed projectile and observe the ejecta and potentially the crater both with remote sensing instruments on the main space craft and from ground-based and satellite telescopes in order to get information about the composition, strength and vertical structure below the surface (A'Hearn et al. 2005). In addition, important observations were made of the nucleus prior to and after the impact of a more general nature, independent of the impact from optical and infrared imaging of the nucleus and nearby gas and dust coma. Evidence from the Deep Impact spacecraft (Groussin et al. 2007) indicates that the nucleus has an extremely low thermal conductivity and the nearly black-body surface temperature penetrates only a few centimeters. Therefore, although subsolar temperatures are in excess of 300 K, the exiting water vapor temperature is close to the vacuum sublimation temperature ~ 190 – 200 K. Measurements and models are coming to a consistent picture. The 200 K sublimation temperature originates a few centimeters below a highly porous and dark refractory layer but does not thermally accommodate to it, explaining the ~ 700 m/s initial gas velocity (Gombosi et al. 1985; Crifo 1987; Combi et al. 2004), consistent with a porous rotating nucleus (Davidsson and Skorov 2002, 2004).

Comet atmospheres are complex since the sublimation is not uniform, gas velocities are not constant, and the production rates can vary by 6–8 orders of magnitude. The simplest model for characterizing the various regimes is a spherical source expanding at a constant velocity for which the gas density is:

$$n = S/(4\pi vr^2),$$

where S is the global production rate, v is the outflow speed and r the distance from the center of the nucleus. Using a collision cross section σ , an expression, analogous to the exobase, is obtained by setting the mean free path equal to the distance to the center of the nucleus (Whipple and Huebner 1976). Therefore, the exobase distance, or collision zone radius, R_{coll} , is: $R_{\text{coll}} = S\sigma/4\pi v$. Gas production rates vary widely from comet to comet and with heliocentric distance, and thus the exobase also varies widely, as shown in Table 1.

The structure of the atmosphere depends on the relative size of R_{coll} and the length scales for photodissociation and photoionization. These length scales vary inversely as the square of the comet's heliocentric distance, except near the nucleus where optical depth effects can be important. They also depend on velocities that vary with species, S and r (Bockelée-Morvan and Crovisier 1987; Combi 1987, 1989; Ip 1989). Species produced below R_{coll} can be collisionally quenched while those produced above R_{coll} can escape, similar to the hot coronae around the planets described earlier. The latter are described by Monte Carlo

simulations as discussed earlier for the planets and satellites. Even in moderately bright comets the abundance of hot species is large enough to be the principal heat source for the extended atmosphere.

An important complication is suprathermal H. As discussed earlier, heavy products from photodissociation have excess energies $\lesssim 2\text{--}4$ eV, yielding velocities in the range of 1–3 km/s. One to three collisions with the ambient molecules can accommodate a heavy hot species to the local flow. However, H atoms from the photodissociation of H₂O and OH have ~ 1.5 to 2.5 eV, yielding velocities ~ 8 to 20 km/s, requiring ~ 10 or more collisions to accommodate. Slow thermalization of hot H is important for the spatial distribution in the outer exosphere, and is heating the nearly collisionally thick inner coma, increasing its outflow speed. While heavy molecule outflow speeds are ~ 0.7 km/s by 1–2 radii from the nucleus, the outflow speed can vary up to ~ 1 km/s for a Halley-class comet when it is at ~ 1 AU (Lämmerzahl et al. 1987) and up to $\gtrsim 2$ km/s when the production rate is high, as for 1995 O1 Hale-Bopp, or for 1996 B2 Hyakutake and 2006 P McNaught near perihelion. The criterion is the ratio between the dissociation scale length and R_{coll} .

Outflow speeds have been obtained using radio measurements of OH Doppler-broadened line profiles (Tseng et al. 2007). Figure 9a gives these speeds as a function of distance from the nucleus estimated from the effective aperture size. The larger expansion speeds correspond to higher production rates and small heliocentric distances, where the dissociation scale lengths become small compared with R_{coll} . A comparison of hybrid fluid/kinetic models for the expansion speeds of the productive comet C/1995 O1 Hale-Bopp is shown in Fig. 9b for different heliocentric distances (Combi et al. 1999). The variations are reasonably well reproduced, but with the calculated velocities and temperatures systematically larger. The IR cooling, optical trapping and photodissociation branching ratios are the most uncertain aspects (Combi et al. 2004).

The complementary part of this problem is seen in Fig. 10 via the Lyman-alpha line profile in comet C/1996 B2 Hyakutake (Combi et al. 1998). The heavy line shows the model convolved with the GHRS spectral function and the observations (triangles). The model, binned at 1 km/s intervals, is the thin line on which the separate components are seen. The central core comes from H produced in the inner coma merging with the suprathermal H produced from the OH and H₂O outside the collision region.

A hydrodynamic model including corrections for the free expansion of light species (Marconi and Mendis 1983; Ip 1983b; Huebner and Keady 1984) and a hybrid kinetic/hydrodynamic model were used in which the light species were modeled by a test particle method and the heavy-molecule coma is modeled by hydrodynamics (Bockelée-Morvan and Crovisier 1987; Combi 1987; Ip 1989). DSMC models were subsequently carried out for a multispecies coma (Combi 1996) and for transitional and non-spherical flows near weak comets (Crifo et al. 2002, 2005; Skorov et al. 2004, 2006; Tenishev et al. 2008).

The large H coma of comet Hale-Bopp at perihelion (FOV $\sim 40^\circ$), obtained using the SWAN all-sky Ly- α camera on the SOHO (Combi et al. 2000), is due to the large production rate ($> 10^{31}$ s⁻¹). A larger fraction of the H are slowed and thermalized than in bright comets, resulting in slower expansion of the H coma but faster expansion of the heavy atom coma (Tseng et al. 2007). Therefore C and O have also been observed in wide-field images and imaging spectrometers (Feldman et al. 2004). Figure 11 shows the large coma in the forbidden emission from the O(¹D) that are produced by photodissociation of H₂O and OH giving a direct measure of the spatial distributions of these parents. Such observations have been useful in determining water production rates (Biermann and Trefftz 1964; Delsemme and Combi 1979; Festou and Feldman 1981; DiSanti and Fink 1991).

In spite of considerable progress, certain branching ratios and energetics remain to be explained (Morgenthaler et al. 2001; Cochran and Cochran 2001; Cochran 2007). In the

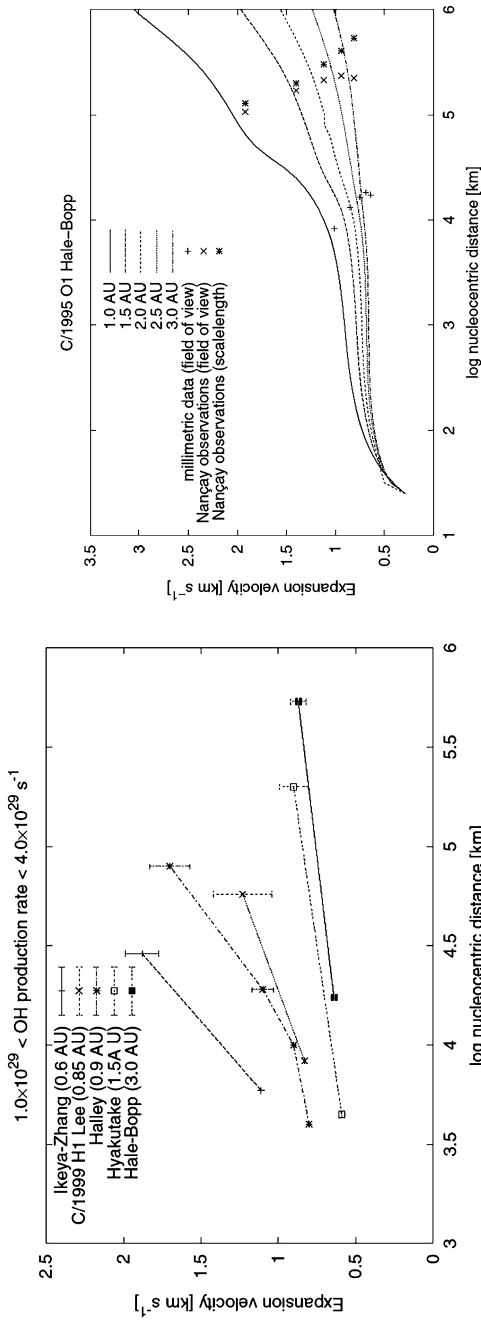


Fig. 9 (a) Expansion speeds in comets from radio observations of Doppler broadened OH (Tseng et al. 2007). Lines toward the upper left tend to larger production rates and smaller heliocentric distances. (b) Expansion speeds in C/1995 O1 (Hale-Bopp) for different heliocentric and nucleocentric distances compared with hybrid kinetic/hydrodynamics models (Combi et al. 2000). Points from Tseng et al. (2007): nucleocentric distance in km is estimated from the telescope aperture size projected on the sky plane

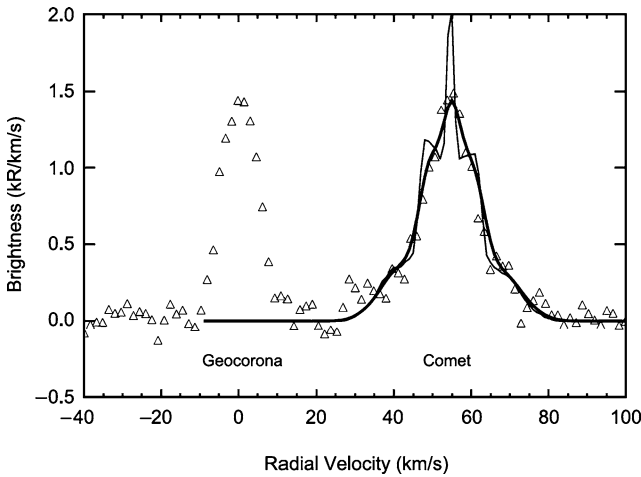


Fig. 10 H Lyman-alpha line profile in C/1996 B2 (Hyakutake). *Triangles*: line profile of the optically thin region of the coma obtained with the GHRs instrument on HST with the small science aperture located 111,000 km sunward of the nucleus. *Thin line*: intrinsic emission at high spectral resolution (1 km/s); *thick line*: model convolved with the instrument spectral function (~ 4 km/s resolution). H emission in the geocorona: at 0 km/s to the left; comet's emission is Doppler shifted to 55 km/s relative geocentric velocity (Feldman et al. 2004; Combi et al. 1998)

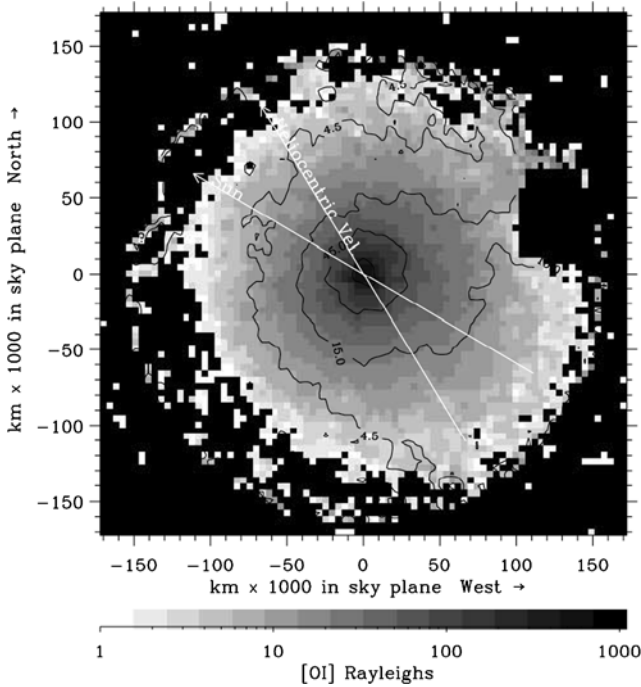


Fig. 11 Wide-field images of the [O I] 6300 Å emission plus continuum from comet C 1996 B2 Hyakutake. *Gray scale*: [O I] emission; *contours*: dust continuum. Emission is from $O(^1D)$ produced by dissociation of H_2O ($\lesssim 10^5$ km) and OH ($\gtrsim 10^5$ km) (Morgenthaler et al. 2007)

absence of better molecular data, it is still problematic to obtain consistent production rates using observations of H₂O (Dello Russo et al. 2006), OH in the near UV from the ground (Schleicher et al. 1998) or from space (Weaver et al. 1999), in the radio from the ground (G erard et al. 1998) or microwave from space (Bensch et al. 2004), H from the ground (Smyth et al. 1993) or from space (Combi et al. 2000), and [O I] (Fink and Hicks 1996; Fink et al. 1991; Morgenthaler et al. 2001, 2007; Cochran 2007).

6 Summary

The physics and chemistry that describe the formation of a corona and the escape rate from a planetary body are critical aspects of aeronomy. They are of interest in understanding present day observations of upper atmospheres, exospheres, extended neutral clouds and pick-up ions source rates. Accurate descriptions of the corona and the present rate of escape are also absolutely necessary in order to attempt to extrapolate back in time and describe the evolution of a planet's atmosphere.

The fundamental physical and chemical processes that determine planetary escape are reasonably well understood with the possible exception of slow hydrodynamic escape. It is described in detail here, since describing the transition region of an atmosphere is still problematic and there is controversy as to when heating by thermal conduction from below becomes an effective escape process. In addition, the data base for cross sections and branching ratios is inadequate for most of the bodies discussed above (Huestis et al. 2008).

Although enormous progress has been made, escape and corona formation are not yet well described for any of the bodies discussed. This is the case for a number of reasons. A principal reason is that on all non-magnetized bodies, the flow through the transition region of the ambient ions, the pick-up ions and the ionospheric ions is critical, but fully self-consistent models of the plasma flow and the interaction of the ionosphere with the ambient fields are just becoming available. What is especially of interest for extrapolating to earlier epochs at Mars are descriptions of the plasma flow and the ion and neutral escape rates vs. the various solar wind conditions. Some progress has been made recently. For instance, the ambitious model of Chaufray et al. (2007) for Mars does treat the interaction and the atmosphere iteratively, and calculates both neutral and ion loss for solar minimum and maximum, but it uses a simplified model atmosphere and the hybrid interaction model does not have sufficient spatial resolution in the exobase region. More importantly, although the solar EUV was varied, the effect of changes in the solar wind pressure that are applicable to earlier solar conditions was not treated. At Titan, although the interaction of the upper atmosphere with the magnetosphere is not well modeled, a good description of the structure of the thermosphere and corona near the exobase is evolving due to the availability of extensive Cassini data (e.g., De La Haye et al. 2007a, 2007b; Cui et al. 2008). Simulations of this structure are being carried out that will be able to test models for escape.

For all the bodies discussed, the principal focus should be on improving the description of the plasma flow around and through the exobase region of each planetary body. Since iterative models are now being developed, and new in-situ spacecraft data is becoming available, extensive progress is expected in the next few years. However, confidence in the modeling will require a concomitant improvement in the molecular data base.

Acknowledgements Support is acknowledged support from NASA's Planetary Atmospheres Program [REJ grant NNG06GC09G; MRC grant NNG06GF51G; JLF grant NN606GF216], by VIS from RFFI Grant 08-02-00263, W.-H. Ip from NSC 96-2752-M-008-011-PAE and NSC 96-2111-M-008-010.

References

- M.F. A'Hearn et al., *Science* **310**, 258–264 (2005)
- J.M. Ajello, M. Ciocca, *J. Geophys. Res.* **101**, 18,953–18,960 (1996)
- C.J. Alexander, C.T. Russell, *Geophys. Res. Lett.* **12**, 369 (1985)
- D.E. Anderson, C.W. Hord, *J. Geophys. Res.* **76**, 6666–6673 (1971)
- D.E. Anderson Jr., *J. Geophys. Res.* **81**, 1213–1216 (1976)
- M. Armenante, V. Santoro, N. Spinelli, F. Vanoli, *Int. J. Mass Spectrom. Ion Proc.* **64**, 265–273 (1985)
- W.I. Axford, *J. Geophys. Res.* **73**, 6855 (1968)
- S. Barabash, A. Fedorov, R. Lundin, J.-A. Sauvaud, *Science* **315**, 501 (2007a)
- S. Barabash et al., *Nature* **450**, 650–653 (2007b)
- D.D. Barbosa, *Icarus* **72**, 53–56 (1987)
- A.R. Barakat, J. Lemaire, *Phys. Rev. A* **42**(6), 3291–3302 (1990)
- R. Bauske, A.F. Nagy, T.I. Gombosi, D.L. De Zeeuw, K.G. Powell, J.G. Luhmann, *J. Geophys. Res.* **103**(A10), 23625–23638 (1998)
- F. Bensch, E.A. Bergin, D. Bockelée-Morvan, G.J. Melnick, N. Biver, *Astrophys. J.* **609**, 1164–1169 (2004)
- J.-L. Bertaux, J. Blamont, M. Marcelin, *Planet. Space Sci.* **26**, 817–831 (1978)
- L. Biermann, D. Trefftz, *Z. Astrophys.* **59**, 1–28 (1964)
- G.A. Bird, *Molecular Gas Dynamics and the Direct Simulation of Gas Flows* (Clarendon, Oxford, 1994)
- D.V. Bisikalo, V.I. Shematovich, J.-C. Gerard, *J. Geophys. Res.* **100**, 3715–3720 (1995)
- D. Bockelée-Morvan, J. Crovisier, in *Proceedings, Symposium on The Diversity and Similarity of Comets*. ESA SP-278 (1987)
- S. Bougher et al., *Space Sci. Rev.* (2008, this issue)
- M. Bouhram, R.W. Johns, J.-J. Berthelier, J.-M. Illiano, R.L. Tokar, D.T. Young, F.J. Cray, *Geophys. Res. Lett.* **33**, L05106 (2006). doi:[10.1029/2005GL025011](https://doi.org/10.1029/2005GL025011)
- R.T. Brinkmann, *Science* **174**, 944–945 (1971)
- R.A. Brown, in *IAU Symp. 65: Exploration of the Planetary System* (1974), pp. 527–531
- R.A. Brown, *Astrophys. J.* **244**, 1072 (1981)
- W.L. Brown et al., *Nucl. Instrum. Methods* **198**, 1 (1982)
- M.E. Brown, R.E. Hill, *Nature* **380**, 229–231 (1996)
- M.E. Brown, *Icarus* **151**, 190–195 (2001)
- M.H. Burger, N.M. Schneider, J.K. Wilson, *Geophys. Res. Lett.* **26**, 3333–3336 (1999)
- M.H. Burger, R.E. Johnson, *Icarus* **171**, 557–560 (2004)
- M.H. Burger, E.C. Sittler Jr., R.E. Johnson, H.T. Smith, O.J. Tucker, V.I. Shematovich, *J. Geophys. Res.* **112**, A06219 (2007). doi:[10.1029/2006JA012086](https://doi.org/10.1029/2006JA012086)
- R.W. Carlson, *Science* **283**, 821–821 (1999)
- E. Carlsson et al., *Icarus* **182**, 320–328 (2006)
- T.A. Cassidy, R.E. Johnson, M.A. McGrath, M.C. Wong, J.F. Cooper, *Icarus* **191**, 755–764 (2007)
- J.W. Chamberlain, *Planet. Space Sci.* **11**, 901 (1963)
- J.W. Chamberlain, *Astrophys. J.* **155**, 711 (1969)
- J.W. Chamberlain, F.J. Campbell, *Astrophys. J.* **149**, 687–705 (1967)
- J.W. Chamberlain, D.M. Hunten, *Theory of Planetary Atmospheres* (Academic Press, New York, 1987)
- E. Chassefière, F. Leblanc, *Planet. Space Sci.* **52**, 1039 (2004)
- E. Chassefière, F. Leblanc, B. Langlais, *Planet. Space Sci.* **55**, 343 (2007)
- J.-Y. Chaufray, R. Modolo, F. Leblanc, G.M. Chanteur, R.E. Johnson, J.G. Luhmann, *J. Geophys. Res.* **112** (2007). doi:[10.1029/2007JE002915](https://doi.org/10.1029/2007JE002915)
- J.-Y. Chaufray, J.-L. Bertaux, E. Quémerais, F. Leblanc, *Icarus* **195**, 598–613 (2008).
- F. Cipriani, F. Leblanc, J.J. Berthelier, *J. Geophys. Res.* E07001 (2007). doi:[10.1029/2006JE002818](https://doi.org/10.1029/2006JE002818)
- A.J. Coates et al., *Geophys. Res. Lett.* **32**, L14S09 (2005). doi:[10.1029/2005GL022694](https://doi.org/10.1029/2005GL022694)
- A.L. Cochran, American Astronomical Society, DPS Meeting, #39, #53.09 (2007)
- A.L. Cochran, W.D. Cochran, *Icarus* **154**, 381–390 (2001)
- M.R. Combi, *Icarus* **71**, 178–191 (1987)
- M.R. Combi, *Icarus* **81**, 41–50 (1989)
- M.R. Combi, *Icarus* **123**, 207–226 (1996)
- M.R. Combi, M.E. Brown, P.D. Feldman, H.U. Keller, R.R. Meier, W.H. Smyth, *Astrophys. J.* **494**, 816–821 (1998)
- M.R. Combi, A.L. Cochran, W.D. Cochran, D.L. Lambert, C.M. Johns-Krull, *Astrophys. J.* **512**, 961–968 (1999)
- M.R. Combi, A.A. Reinard, J.-L. Bertaux, E. Quémérais, T. Mäkinen, *Icarus* **144**, 191–202 (2000)
- M.R. Combi, W.M. Harris, W.H. Smyth, in *Comets II*, ed. by M.C. Festou et al. (University of Arizona Press, Tucson, 2004), pp. 523–552

- J.E.P. Connerney, J.H. Waite, *Nature* **312**, 136 (1984)
- A.F. Cook, A.F. Franklin, *Astrophys. J.* **75**, 195 (1970)
- J.F. Cooper, *J. Geophys. Res.* **88**, 3945–3954 (1983)
- P.C. Cosby, *J. Chem. Phys.* **98**, 9560–9569 (1993)
- T.E. Cravens, C.N. Keller, B. Ray, *Planet. Space Sci.* **45**, 889 (1997)
- T.E. Cravens, A. Hoppe, S.A. Ledvina, S. McKenna-Lawlor, *J. Geophys. Res.* **107**, 7-1–7-10 (2002). doi:[10.1029/2001JA000125](https://doi.org/10.1029/2001JA000125)
- J.F. Crifo, *Astron. Astrophys.* **187**, 438–450 (1987)
- J.F. Crifo, G.A. Loukianov, A.V. Rodionov, G.O. Khanlarov, V.V. Zakharov, *Icarus* **156**, 249–268 (2002)
- J.F. Crifo, G.A. Loukianov, A.V. Rodionov, G.O. Khanlarov, V.V. Zakharov, *Icarus* **176**, 192–219 (2005)
- J. Cui, R.V. Yelle, K. Volk, *J. Geophys. Res.* (2008, in press)
- J.N. Cuzzi et al., *Space Sci. Rev.* **104**, 209 (2002)
- B.J.R. Davidsson, Y.V. Skorov, *Icarus* **159**, 239–258 (2002)
- B.J.R. Davidsson, Y.V. Skorov, *Icarus* **168**, 163–185 (2004)
- V. De La Haye, J.H. Waite Jr., R.E. Johnson, R.V. Yelle, T.E. Cravens, J.G. Luhmann, W.T. Kasprzak, D.A. Gell, B. Magee, F. Leblanc, M. Michael, S. Jurac, I.P. Robertson, *J. Geophys. Res.* **112**(A7), A07309 (2007a). doi:[10.1029/2006JA012222](https://doi.org/10.1029/2006JA012222)
- V. De La Haye, J.H. Waite Jr., T.E. Cravens, A.F. Nagy, R.V. Yelle, R.E. Johnson, S. Lebonnois, I.P. Robertson, *Icarus* **191**, 236–250 (2007b)
- N. Dello Russo, M.J. Mumma, M.A. DiSanti, K. Magee-Sauer, E.L. Gibb, B.P. Bonev, I.S. McLean, L.-H. Xu, *Icarus* **184**, 255–276 (2006)
- A.H. Delsemme, M.R. Combi, *Astrophys. J.* **228**, 330–337 (1979)
- H.G. Demars, A.R. Barakat, R.W. Schunk, *J. Atmos. Sol. Terr. Phys.* **55**, 1583–1598 (1993)
- M.A. DiSanti, U. Fink, *Icarus* **91**, 105–111 (1991)
- T.M. Donahue, J.H. Hoffman, R.R. Hodges, A.J. Watson, *Science* **216**, 630–633 (1982)
- M.K. Dougherty, K.K. Khurana, F.M. Neubauer, C.T. Russell, J. Saur, J.S. Leisner, M.E. Burton, *Science* **311**, 1406–1409 (2006)
- S.T. Durrance, P.D. Feldman, H.A. Weaver, *Astrophys. J.* **267**, L125 (1983)
- S.T. Durrance, P.D. Feldman, W.P. Blair, A.F. Davidsen, G.A. Kriss, J.W. Kruk, K.S. Long, H.W. Moos, *Astrophys. J.* **447**, 408 (1995)
- L.W. Esposito, J.E. Colwell, K. Larsen et al., *Science* **307**, 1251 (2005)
- A.J. Farmer, P. Goldreich, *Icarus* **179**, 535 (2005)
- A.J. Farmer, P. Goldreich, *Icarus* **188**, 108–119 (2007)
- L.M. Feaga, M.F. A'Hearn, J.M. Sunshine, O. Groussin, T.L. Farnham, *Icarus* **190**, 345 (2007)
- P.D. Feldman, M.A. McGrath, D.F. Strobel, H.W. Moos, K.D. Retherford, B.C. Wolven, *Astrophys. J.* **535**, 1085–1090 (2000)
- P.D. Feldman, A.L. Cochran, M.R. Combi, in *Comets II*, ed. by M.C. Festou, H.U. Keller, H.A. Weaver (University of Arizona Press, Tucson, 2004), pp. 425–447
- M.C. Festou, P.D. Feldman, *Astron. Astrophys.* **103**, 154–159 (1981)
- U. Fink, M.R. Combi, M.A. DiSanti, *Astrophys. J.* **383**, 356–371 (1991)
- U. Fink, M.D. Hicks, *Astrophys. J.* **459**, 729–743 (1996)
- J.L. Fox, *Adv. Space Res.* **5**, 165 (1985)
- J.L. Fox, *Planet. Space Sci.* **34**, 1252 (1986)
- J.L. Fox, *J. Geophys. Res.* **98**, 3297–3310 (1993)
- J.L. Fox, *Geophys. Res. Lett.* **24**, 2901 (1997)
- J.L. Fox, *Icarus* **192**, 296–301 (2007)
- J.L. Fox, F.M. Bakalian, *J. Geophys. Res.* **106**, 28785 (2001)
- J.L. Fox, J.H. Black, *Geophys. Res. Lett.* **16**, 291 (1989)
- J.L. Fox, A. Dalgarno, *J. Geophys. Res.* **84**, 7315–7333 (1979)
- J.L. Fox, A. Dalgarno, *J. Geophys. Res.* **88**, 9027–9032 (1983)
- J.L. Fox, A. Dalgarno, *J. Geophys. Res.* **90**, 7557–7567 (1985)
- J.L. Fox, A. Hać, *J. Geophys. Res.* **102**, 24,005–24,011 (1997a)
- J.L. Fox, A. Hać, *J. Geophys. Res.* **102**, 9191–9204 (1997b)
- J.L. Fox, L.J. Paxton, *J. Geophys. Res.* **110**, A01311 (2005). doi:[10.1029/2004JA010813](https://doi.org/10.1029/2004JA010813)
- E. Gérard, J.P. Crovisier, N. Colom, D. Biver, D. Bockelée-Morvan, H. Rauer, *Planet. Space Sci.* **46**, 569–577 (1998)
- C.K. Goertz, G. Morfill, *Icarus* **43**, 219 (1983)
- T.I. Gombosi, T.E. Cravens, A.F. Nagy, *Astrophys. J.* **293**, 328–341 (1985)
- O. Groussin, M.F. A'Hearn, J.-Y. Li, P.C. Thomas, J.M. Sunshine, C.M. Lisse, K.J. Meech, T.L. Farnham, L.M. Feaga, W.A. Delamere, *Icarus* **187**, 16–25 (2007)
- S.L. Guberman, A. Giusti-Suzor, *J. Chem. Phys.* **95**, 2602–2613 (1991)

- H. Gunell et al., *Icarus* **182**(2), 431–438 (2006)
- P.K. Haff, A. Eviatar, G.L. Siscoe, *Icarus* **56**, 426 (1983)
- D.T. Hall, D.F. Strobel, P.D. Feldman, M.A. McGrath, H.A. Weaver, *Nature* **373**, 677–679 (1995)
- D.T. Hall, P.D. Feldman, J.B. Holberg, M.A. McGrath, *Science* **272**, 516 (1996)
- D.T. Hall, P.D. Feldman, M.A. McGrath, D.F. Strobel, *Astrophys. J.* **499**, 475–481 (1998)
- C.J. Hansen, D. Shemansky, A. Hendrix, *Icarus* **176**, 305–315 (2005)
- C.J. Hansen, L. Esposito, A.I.F. Stewart, J. Colwell, A. Hendrix, W. Pryor, D.E. Shemansky, R. West, *Science* **311**, 1422 (2006)
- W.B. Hanson, S. Sanatani, D.R. Zuccaro, *J. Geophys. Res.* **82**, 4351 (1977)
- E.M. Harnett, R.M. Winglee, *J. Geophys. Res.* **111**, A09213 (2006). doi:[10.1029/2006JA011724](https://doi.org/10.1029/2006JA011724)
- R.E. Hartle, *Planet. Space Sci.* **21**, 12123–12137 (1973)
- R.R. Hodges, *J. Geophys. Res.* **98**, 10,833–10,838 (1993)
- R.R. Hodges, *J. Geophys. Res.* **99**, 23,229–23,247 (1994)
- R.R. Hodges, *J. Geophys. Res.* **105**, 6971 (2000)
- W.F. Huebner, J.J. Keady, in *Cometary Exploration*, ed. by T. Gombosi (Budapest, 1984), pp. 165–183
- D.L. Huestis et al., *Space Sci. Rev.* (2008, this issue)
- D.M. Hunten, A.J. Watson, *Icarus* **51**, 665–667 (1982)
- W.-H. Ip, *J. Geophys. Res.* **88**, 819 (1983a)
- W.-H. Ip, *Astrophys. J.* **264**, 726–732 (1983b)
- W.-H. Ip, *J. Geophys. Res.* **89**, 395 (1984a)
- W.-H. Ip, *J. Geophys. Res.* **89**, 3829 (1984b)
- W.-H. Ip, *Icarus* **76**, 135–145 (1988)
- W.-H. Ip, *Astrophys. J.* **343**, 946–952 (1989)
- W.-H. Ip, *J. Geophys. Res.* **17**, 2289–2292 (1990)
- W.-H. Ip, *Icarus* **115**, 295–303 (1995)
- W.-H. Ip, *Icarus* **126**, 42 (1997)
- W.-H. Ip, *Planet. Space Sci.* **48**, 775 (2000)
- W.-H. Ip, *Geophys. Res. Lett.* **32**, L13204 (2005). doi:[10.1029/2004GL022217](https://doi.org/10.1029/2004GL022217)
- R.E. Johnson, *J. Geophys. Res. Lett.* **5**, 989 (1978)
- R.E. Johnson, *Energetic Charged Particle Interaction with Atmospheres and Surfaces* (Springer, New York, 1990)
- R.E. Johnson, *Icarus* **111**, 65–72 (1994)
- R.E. Johnson, *Icarus* **143**, 429–433 (2000)
- R.E. Johnson, *Astrophys. J.* **609**, L99–L102 (2004)
- R.E. Johnson, *Proc. R. Soc. (Lond.)* (2008, in press)
- R.E. Johnson, J.G. Luhmann, *J. Geophys. Res.* **103**, 3649–3653 (1998)
- R.E. Johnson, T.I. Quickenden, *J. Geophys. Res.* **102**, 10985 (1997)
- R.E. Johnson, L.J. Lanzerotti, W.L. Brown, *Nuclear Instrum. Methods* **198**, 147 (1982)
- R.E. Johnson, M.K. Pospieszalska, E.C. Sitler Jr., A.F. Cheng, L.J. Lanzerotti, E.M. Sieveka, *Icarus* **77**, 311 (1989)
- R.E. Johnson, D. Schnellenberger, M.C. Wong, *J. Geophys. Res.* **105**, 1659 (2000)
- R.E. Johnson, M. Liu, C. Tully, *Planet. Space Sci.* **50**, 123–128 (2002)
- R.E. Johnson, T.I. Quickenden, P.D. Cooper, A.J. McKinley, C. Freeman, *Astrobiology* **3**, 823–850 (2003)
- R.E. Johnson et al., *Icarus* **180**, 393 (2006)
- R.E. Johnson et al., in *Europa*, ed. by R. Pappalardo et al. (2008, in press)
- S. Jurac, J.D. Richardson, *J. Geophys. Res.* **110**, A09220 (2005). doi:[10.1029/2004JA010635](https://doi.org/10.1029/2004JA010635)
- S. Jurac, M.A. McGrath, R.E. Johnson, J.D. Richardson, V.M. Vasyliunas, A. Eviatar, *Geophys. Res. Lett.* **29**(24), 2172 (2002). doi:[10.1029/2002GL015855](https://doi.org/10.1029/2002GL015855)
- K. Kabin, B.D. Shizgal, *J. Geophys. Res.* **107**(E7), 5053 (2002). doi:[10.1029/2000JE001479](https://doi.org/10.1029/2000JE001479)
- E. Kallio, H. Koskinen, *J. Geophys. Res.* **104**, 557 (1999)
- E. Kallio, J.G. Luhmann, S. Barabash, *J. Geophys. Res.* **102**, 22,183–22,197 (1997)
- E. Kallio, J.G. Luhmann, J.G. Lyon, *J. Geophys. Res.* **103**(A3), 4753–4754 (1998)
- G.M. Keating et al., *Science* **279**, 1672–1676 (1998)
- D. Kella, P.J. Johnson, H.B. Pedersen, L. Vejby-Christensen, L.H. Andersen, *Science* **276**, 1530–1533 (1997)
- V. Kharchenko, A. Dalgarno, B. Zygelman, J.-H. Yee, *J. Geophys. Res.* **103**, 24899–24906 (2000)
- J. Kim, A.F. Nagy, J.L. Fox, T.E. Cravens, *J. Geophys. Res.* **103**, 29339 (1998)
- Y.H. Kim, S. Son, *J. Korean Astron. Soc.* **33**, 127–135 (2000)
- Y.H. Kim, S. Son, J. Kim, *J. Korean Astron. Soc.* **34**, 25–29 (2001)
- M.G. Kivelson, K.K. Khurana, R.J. Walker, J. Warnecke, C.T. Russell, J.A. Linker, D.J. Southwood, C. Polansky, *Science* **274**, 396–398 (1996)
- A.J. Kliore, D.P. Hinson, F.M. Flasar, A.F. Nagy, *Science* **277**, 355–358 (1997)

- G. Kotova, M. Verigin, A. Remizov, N. Shutte, J. Slavin, K. Szego, M. Tatrallyay, H. Rosenbauer, V.A. Krasnopolsky, D.P.J. Cruikshank, *Geophys. Res.* **100**, 21,271–21,286 (1995)
- G. Kotova, M. Verigin, A. Remizov, N. Shutte, H. Rosenbauer, S. Livi, K. Szego, M. Tatrallyay, J. Slavin, J. Lemaire, K. Schwingenschuh, T.-L. Zhang, *Geophys. Res.* **102**, 2165–2174 (1997)
- V.A. Krasnopolsky, *J. Geophys. Res.* **104**, 5955–5962 (1999)
- M.A. Krestyanikova, V.I. Shematovich, *Sol. Syst. Res.* **39**, 22 (2005)
- M.A. Krestyanikova, V.I. Shematovich, *Sol. Syst. Res.* **40**, 384–392 (2006)
- S.M. Krimigis et al., *Nature* **415**, 994–996 (2002)
- S.M. Krimigis et al., *Science* **307**, 1270 (2005)
- A.M. Krymskii, T.K. Breus, *J. Geophys. Res.* **101**, 7599 (1996)
- S. Kumar, *Icarus* **61**, 101–123 (1985)
- A. Lagg, N. Krupp, J. Woch, S. Livi, B. Wilken, D.J. Williams, *Geophys. Res. Lett.* **25**, 4039–4042 (1998)
- A. Lagg, N. Krupp, J. Woch, D.J. Williams, *Geophys. Res. Lett.* **30** (2003). doi:[10.1029/2003GL017214](https://doi.org/10.1029/2003GL017214). 1556
- H. Lammer, S.J. Bauer, *J. Geophys. Res.* **96**, 1819–1825 (1991)
- H. Lammer, W. Stumptner, G.J. Molina-Cuberos, S.J. Bauer, T. Owen, *Planet. Space Sci.* **48**, 529–543 (2000)
- H. Lammer, H.I.M. Lichtenegger, H.K. Biernat, N.V. Erkaev, I.L. Arshukova, C. Kolb, H. Gunell, A. Lukyanov, M. Holmstrom, S. Barabash, T.L. Zhang, W. Baumjohann, *Planet. Space Sci.* **54**, 1445–1456 (2006)
- H. Lammer et al., *Space Sci. Rev.* (2008, this issue)
- P. Lämmerzahl, D. Krankowsky, R.R. Hodges, U. Stubbemann, J. Woweries, I. Herrwerth, J.J. Berthelier, J.M. Illiano, P. Eberhardt, U. Dolder, W. Schulte, J.H. Hoffman, *Astron. Astrophys.* **187**, 169–173 (1987)
- L.D. Landau, E.M. Lifshitz, *Fluid Mechanics*, 2nd ed., vol. 6 (Pergamon Press, 1987), p. 539
- F. Leblanc, R.E. Johnson, *Planet. Space Sci.* **49**, 645 (2001)
- F. Leblanc, R.E. Johnson, *J. Geophys. Res.* **107** (2002a). doi:[10.1029/2000JE001473](https://doi.org/10.1029/2000JE001473)
- F. Leblanc, R.E. Johnson, M.E. Brown, *Icarus* **159**, 132–144 (2002b)
- F. Leblanc, A.E. Potter, R.M. Killen, R.E. Johnson, *Icarus* **178**, 367–385 (2005)
- F. Leblanc, J.Y. Chaufray, O. Witasse, J. Lilensten, J.-L. Bertaux, *J. Geophys. Res.* **111**, E09S11 (2006). doi:[10.1029/2005JE002664](https://doi.org/10.1029/2005JE002664)
- F. Leblanc, J.Y. Chaufray, J.L. Bertaux, *Geophys. Res. Lett.* **34**, L02206 (2007). doi:[10.1029/2006GL028437](https://doi.org/10.1029/2006GL028437)
- S.A. Ledvina, T.E. Cravens, K. Kecskeméty, *J. Geophys. Res.* **110** (2005). CiteID A06211
- S.A. Ledvina et al., *Space Sci. Rev.* (2008, this issue)
- B.R. Lewis, S.T. Gibson, W. Zhang, H. Lefebvre-Brion, J.-M. Robbe, *J. Chem. Phys.* **122**, 144302 (2005)
- H.I.M. Lichtenegger, H. Lammer, Y.N. Kulikov, S. Kazeminejad, G.H. Molina-Cuberos, R. Rodrigo, B. Kazeminejad, G. Kirchengast, *Space Sci. Rev.* (2007, in press). doi:[10.1007/s11214-006-9082-1](https://doi.org/10.1007/s11214-006-9082-1)
- M.W. Liemohn, J.L. Fox, A.F. Nagy, X. Fang, *J. Geophys. Res.* **109**, A10307 (2004). doi:[10.1029/2004JA010643](https://doi.org/10.1029/2004JA010643)
- R.W. Locht, M. Davister, *Int. J. Mass Spectrom. Ion Proc.* **144**, 105–129 (1995)
- J.G. Luhmann, *J. Geophys. Res.* **101**, 7603 (1996)
- J.G. Luhmann, J.U. Kozyra, *J. Geophys. Res.* **96**, 5457–5468 (1991)
- J.G. Luhmann, R.E. Johnson, M.H.G. Zhang, *Geophys. Res. Lett.* **19**, 2151 (1992)
- J.G. Luhmann, R.E. Johnson, R.L. Tokar, S.A. Ledvina, T.W. Cravens, *Icarus* **181**, 465 (2006a)
- J.G. Luhmann, S.A. Ledvina, J.G. Lyon, C.T. Russell, *Planet. Space Sci.* **54**, 1482–1495 (2006b)
- J.G. Luhmann, W.T. Kasprzak, C.T. Russell, *J. Geophys. Res.* **112** (2007). doi:[10.1029/2006JE002820](https://doi.org/10.1029/2006JE002820)
- H. Luna, M. Michael, M.B. Shah, R.E. Johnson, C.J. Latimer, J.W. McConkey, *J. Geophys. Res.* **108**(E4), 5033 (2003). doi:[10.1029/2002JE001950](https://doi.org/10.1029/2002JE001950)
- H. Luna, C. McGrath, M.B. Shah, R.E. Johnson, M. Liu, C.J. Latimer, E.C. Montenegro, *Astrophys. J.* **628**, 1086–1096 (2005)
- R. Lundin, S. Barabash, *Planet. Space Sci.* **52**, 1059–1071 (2004)
- R. Lundin, E.M. Dubinin, *Adv. Space Res.* **12**(9), 255 (1992)
- R. Lundin et al., *Nature* **341**, 609 (1989)
- R. Lundin, E.M. Dubinin, S.V. Barabash, H. Koskinen, O. Norberg, N. Pissarenko, A.V. Zakharov, *Geophys. Res. Lett.* **18**, 1059 (1991)
- Y. Ma, A.F. Nagy, *Geophys. Res. Lett.* **34** (2007). doi:[10.1029/2006GL029208](https://doi.org/10.1029/2006GL029208)
- Y. Ma, A.F. Nagy, K.C. Hansen, D.L. DeZeeuw, T.I. Gombosi, K.G. Powell, *J. Geophys. Res.* **107**, 1282 (2002). doi:[10.1029/2002JA009293](https://doi.org/10.1029/2002JA009293)
- Y. Ma, A.F. Nagy, I.V. Sokolov, C.H. Kennel, *J. Geophys. Res.* **109**, A07211 (2004). doi:[10.1029/2003JA010367](https://doi.org/10.1029/2003JA010367)
- Y. Ma et al., *J. Geophys. Res.* **111**, A05207 (2006). doi:[10.1029/2006JA011481](https://doi.org/10.1029/2006JA011481)
- M.L. Marconi, D.A. Mendis, *Astrophys. J.* **273**, 381–396 (1983)

- M.L. Marconi, L. Dagum, W.H. Smyth, *Astrophys. J.* **469**, 393–401 (1996)
- B.H. Mauk, D.G. Mitchell, C. Paranicas, S.M. Krimigis, *Nature* **421**, 920–922 (2003)
- M.B. McElroy, T.Y. Kong, Y.L. Yung, *J. Geophys. Res.* **82**, 4379–4388 (1977)
- M.A. McGrath, R.E. Johnson, *Icarus* **69**, 519 (1987)
- M.A. McGrath, E. Lellouch, D.F. Strobel, P.D. Feldman, R.E. Johnson, in *Jupiter: Satellites, Atmosphere, Magnetosphere*, ed. by F. Bagenal et al. (Cambridge Univ. Press, Cambridge, 2004), pp. 457–483
- M.A. McGrath et al., in *Europa*, ed. by R. Pappalardo et al. (2008, in press)
- S.M.P. McKenna-Lawlor, V. Afonin, Y. Yeroshenko, E. Keppler, E. Kirsch, K. Schwingenschuh, *Planet. Space Sci.* **41**, 373 (1993)
- R.L. McNutt, *Geophys. Res. Lett.* **16**, 1225–1228 (1989)
- M. Mendillo, J. Baumgardner, B. Flynn, J.W. Hughes, *Nature* **348**, 312–314 (1990)
- M. Michael, R.E. Johnson, F. Leblanc, M. Liu, J.G. Luhmann, V. Shematovich, *Icarus* **175**, 263–267 (2005)
- M. Michael, R.E. Johnson, *Planet. Space Sci.* **53**, 1510–1514 (2005)
- R. Modolo, G.M. Chanteur, E. Dubinin, A.P. Matthews, *Ann. Geophys.* **23**, 433 (2005)
- L. Moore, M. Mendillo, *Geophys. Res. Lett.* **34**, L12202 (2007). doi:[10.1029/2007GL029381](https://doi.org/10.1029/2007GL029381)
- L. Moore, A.F. Nagy, A.J. Kliore, I. Mueller-Wodarg, J. Richardson, M. Mendillo, *Geophys. Res. Lett.* **33**, L22202 (2006). doi:[10.1029/2006GL027375](https://doi.org/10.1029/2006GL027375)
- G.E. Morfill, H.M. Thomas, *Icarus* **179**, 539 (2005)
- J. Morgenthaler, W.M. Harris, F. Scherb, C.M. Anderson, R.J. Oliverson, N.E. Doane, M.R. Combi, M.L. Marconi, W.H. Smyth, *Astrophys. J.* **563**, 451–461 (2001)
- J. Morgenthaler, W.M. Harris, M.R. Combi, *Astrophys. J.* **657**, 1162–1171 (2007)
- J.I. Moses, S.F. Bass, *J. Geophys. Res.* **105**, 7013 (2000)
- J.I. Moses, B. Bezard, E. Lellouch, G.R. Gladstone, H. Feuchtgruber, M. Allen, *J. Geophys. Res.* **105**, 7013 (2000)
- J.I. Moses, M.Y. Zolotov, B. Fegley, *Icarus* **156**, 107–135 (2002)
- A.F. Nagy, P.M. Banks, *J. Geophys. Res.* **75**, 6260 (1970)
- A.F. Nagy, T.E. Cravens, *Geophys. Res. Lett.* **15**, 433 (1988)
- A.F. Nagy, T.E. Cravens, J.-H. Yee, A.I.F. Stewart, *Geophys. Res. Lett.* **8**, 629–632 (1981)
- A.F. Nagy, J. Kim, T.E. Cravens, *Ann. Geophys.* **8**, 251 (1990)
- A.F. Nagy, M.W. Liemohn, J.L. Fox, J. Kim, *J. Geophys. Res.* **106**(15), 21,565–21,568 (2001). doi:[10.1029/2001JA000007](https://doi.org/10.1029/2001JA000007)
- H.B. Niemann et al., *Nature* **438**, 779–784 (2005)
- A.O. Nier, M.B. McElroy, *J. Geophys. Res.* **82**, 4341–4349 (1977)
- T.G. Northrop, J.R. Hill, *J. Geophys. Res.* **88**, 6102 (1983)
- E.N. Parker, *Astrophys. J.* **139**, 93–122 (1964)
- L.J. Paxton, *J. Geophys. Res.* **90**, 5089–5096 (1985)
- J. Pearl, R. Hanel, V. Kunde, W. Maguire, K. Fox, S. Gupta, C. Ponnampereuma, F. Raulin, *Nature* **280**, 755–758 (1979)
- T. Penz, I.L. Arshukova, N. Terada, H. Shinagawa, N.V. Erkaev, H.K. Biernat, H. Lammer, *Adv. Space Res.* **36**, 2049–2056 (2005)
- H. Pérez-de-Tejada, *J. Geophys. Res.* **92**, 4713 (1987)
- H. Pérez-de-Tejada, *J. Geophys. Res.* **103**, 31499–31508 (1998)
- J.R. Peterson, A. Le Padellec, H. Danared, G.H. Dunn, M. Larsson, A. Larson, R. Peverall, C. Strömholm, S. Rosén, M. Af Ugglas, W.J. van der Zande, *J. Chem. Phys.* **108**, 1978–1988 (1998)
- R. Peverall, S. Rosen, J.R. Peterson, M. Larsson, A. Al-Khalili, L. Viktor, J. Semaniak, R. Bobbenkamp, A. LePadellec, A.N. Maurellis, W.J. van der Zande, *J. Chem. Phys.* **114**, 6679–6689 (2001)
- V. Pierrard, *Planet. Space Sci.* **51**, 319 (2003)
- C.B. Pilcher, J.H. Fertel, W.H. Smyth, M.R. Combi, *Astrophys. J.* **287**, 427–444 (1984)
- C.C. Porco et al., *Science* **311**, 1393–1401 (2006)
- M.K. Pospieszalska, R.E. Johnson, *Icarus* **93**, 45 (1991)
- M.K. Pospieszalska, R.E. Johnson, *J. Geophys. Res.* **101**, 7565–7573 (1996)
- T.M. Prokop, E.C. Zipf, *EOS Trans. AGU* **63**, 392 (1982)
- J.D. Richardson, *J. Geophys. Res.* **103**, 20,245 (1998)
- R.P. Rohrbaugh, J.S. Nisbet, *J. Geophys. Res.* **78**, 6768–6772 (1973)
- S. Rosen et al., *Phys. Rev. A* **57**, 4462–4471 (1998)
- H. Rosenbauer, N. Shutte, I. Apathy, A. Galeev, K. Gringauz, H. Gruenwaldt, P. Hemmerich, K. Jockers, P. Kiraly, G. Kotova, S. Livi, E. Marsh, A. Richter, W. Riedler, A. Remizov, R. Schwenn, K. Schwingenschuh, M. Steller, K. Szego, M. Verigin, M. Witte, *Nature* **341**, 612 (1989)
- C.T. Russell, J.G. Luhmann, R.J. Strangeway, *Planet. Space Sci.* **54**, 1482–1495 (2006)
- J. Saur, D.F. Strobel, F.M. Neubauer, *J. Geophys. Res.* **103**, 19947–19962 (1998)
- D.G. Schleicher, R.L. Millis, P.V. Birch, *Icarus* **132**, 397–417 (1998)

- N.M. Schneider, J.K. Wilson, J.T. Trauger, D.I. Brown, R.W. Evans, D.E. Shemansky, *Science* **253**, 1394–1397 (1991)
- N.M. Schneider, J.T. Trauger, *Astrophys. J.* **450**, 450 (1995)
- R.W. Schunk, A.F. Nagy, *Ionospheres: Physics, Plasma Physics, and Chemistry* (Cambridge Univ. Press, New York, 2000)
- K. Seki, R.C. Elphic, M. Hirahara, T. Terasawa, T. Mukai, *Science* **291**(5510), 1939–1941 (2001)
- K. Siersen, A. Al-Khalili, M.J. Jensen, I.B. Nielsen, H.B. Petersen, C.P. Safvan, L.H. Andersen, *Phys. Rev. A* **68**, 022708 (2003)
- D.E. Shemansky, P. Matheson, D.T. Hall, H.-T. Hu, T.M. Tripp, *Nature* **363**, 329 (1992)
- V.I. Shematovich, R.E. Johnson, Hot oxygen coronae at terrestrial planets. Talk at 1st European Congress of Planetary Sciences, Berlin, 2006
- V.I. Shematovich, D.V. Bisikalo, J.-C. Gérard, *J. Geophys. Res.* **99**, 23,217 (1994)
- V.I. Shematovich, J.-C. Gerard, D.V. Bisikalo, B. Hubert, *J. Geophys. Res.* **104**, 4287–4295 (1999)
- V.I. Shematovich, R.E. Johnson, M. Michael, J.G. Luhmann, *J. Geophys. Res.* **108**(E8), 5087 (2003). doi:[10.1029/2003JE002094](https://doi.org/10.1029/2003JE002094)
- V.I. Shematovich, D.V. Bisikalo, J.-C. Gerard, *Geophys. Res. Lett.* **32**, L02105 (2005a)
- V.I. Shematovich, R.E. Johnson, J.F. Cooper, M.C. Wong, *Icarus* **173**, 480–498 (2005b)
- H. Shinagawa, *J. Geophys. Res.* **101**, 26911–26920 (1996)
- H. Shinagawa, T.E. Cravens, *J. Geophys. Res.* **94**, 6506 (1989)
- B.D. Shizgal, M.J. Lindenfeld, *J. Geophys. Res.* **87**, 853 (1982)
- B. Shizgal, R. Blackmore, *Planet. Space Sci.* **34**, 279–291 (1986)
- B.D. Shizgal, G.G. Arkos, *Rev. Geophys.* **34**, 483 (1996)
- B.D. Shizgal, *J. Geophys. Res.* **104**, 14,833 (1999)
- T.E. Skinner, S.T. Durrance, *Astrophys. J.* **310**, 966–971 (1986)
- Y.V. Skorov, G.N. Markelov, H.U. Keller, *Sol. Syst. Res.* **38**, 455–475 (2004)
- Y.V. Skorov, G.N. Markelov, H.U. Keller, *Sol. Syst. Res.* **40**, 219–229 (2006)
- H.T. Smith, R.E. Johnson, E.C. Sittler, M. Shappirio, O.J. Tucker, M. Burger, F.J. Crary, D.J. McComas, D.T. Young, *Icarus* **188**, 356–366 (2007)
- W.H. Smyth, M.R. Combi, *Icarus* **126**, 58–77 (1997)
- W.H. Smyth, M.L. Marconi, *J. Geophys. Res.* **105**, 7783–7792 (2000)
- W.H. Smyth, M.L. Marconi, *Icarus* **181**, 510–526 (2006)
- W.H. Smyth, M. Wong, *Icarus* **171**, 171–182 (2004)
- W.H. Smyth, M.L. Marconi, F. Scherb, F.L. Roesler, *Astrophys. J.* **413**, 756–763 (1993)
- J. Spencer et al., *Science* **311**, 1401–1405 (2006)
- J.P. Sprengers, W. Ubachs, K.G.H. Baldwin, *J. Chem. Phys.* **122**, 144301 (2005)
- S.W. Squyres, R.T. Reynolds, P.M. Cassen, *Icarus* **53**, 319 (1983)
- G. Stark, K. Yoshino, P.L. Smith, K. Ito, *J. Quant. Spectrosc. Radiat. Transf.* **103**, 67–73 (2007)
- D.F. Strobel, X. Zhu, M.E. Summers, M.H. Stevens, *Icarus* **120**, 266–289 (1995)
- D.F. Strobel, in *Comparative Aeronomy in the Solar System*, ed. by M. Mendillo, A. Nagy, H. Waite, *Geophys. Monogr. Ser. (Am. Geophys. U., 2002)*, pp. 7–22
- D.F. Strobel, *Icarus* **193**, 588–594 (2008a)
- D.F. Strobel, *Icarus* **193**, 612–619 (2008b)
- W.-L. Tseng, D. Bockelee-Morvan, J. Crovisier, P. Colom, W.-H. Ip, *Astron. Astrophys.* **467**, 729–735 (2007)
- V. Tenishev et al., (2008, in press)
- N. Terada, H. Shinagawa, S. Machida, *Adv. Space Res.* **33**, 161–166 (2004)
- N. Thomas, *Surv. Geophys.* **13**, 91–164 (1992)
- N. Thomas, *Astron. Astrophys.* **313**, 306–314 (1996)
- N. Thomas, F. Bagenal, T.W. Hill, J.K. Wilson, in *Jupiter. The Planet, Satellites and Magnetosphere*, ed. by F. Bagenal (Cambridge Univ. Press, Cambridge, 2004), pp. 561–591
- C. Tian, C.R. Vidal, *J. Chem. Phys.* **108**, 927–936 (1998)
- F. Tian, O.B. Toon, *Geophys. Res. Lett.* **32**, L18201 (2005). doi:[10.1029/2005GL023510](https://doi.org/10.1029/2005GL023510)
- R.L. Tokar et al., *Geophys. Res. Lett.* **32**, L14S04 (2005). doi:[10.1029/2005GL022690](https://doi.org/10.1029/2005GL022690)
- L. Trafton, *Astrophys. J.* **247**, 1125–1140 (1981)
- C. Tully, R.E. Johnson, *Planet. Space Sci.* **49**, 533–537 (2001)
- A. Vidal-Madjar, J.-L. Bertaux, *Planet. Space Sci.* **20**, 1147 (1972)
- A.A. Viggiano, A. Ehlerding, F. Hellberg, R.D. Thomas, V. Zhaunerchyk, W.D. Geppart, H. Montaigne, M. Larsson, M. Kaminska, F. Osterdahl, *J. Chem. Phys.* **122**(22), 226101 (2005)
- D. Vignes et al., *Geophys. Res. Lett.* **27**, 49 (2000)
- J.H. Waite et al., *Science* **308**, 982–986 (2005a)
- J.H. Waite et al., *Science* **307**, 1260–1262 (2005b)
- J.H. Waite et al., *Science* **311**, 1419–1422 (2006)

- J. Warnecke, M.G. Kivelson, K.K. Khurana, D.E. Huddleston, C.T. Russell, *Geophys. Res. Lett.* **24**, 2139 (1997)
- C.C. Watson, P.K. Haff, T.A. Tombrello, in *Proc. Lunar Planet Sci. Conf. 11th* (1980), pp. 2479–2485
- A.J. Watson, T.M. Donahue, J.C.G. Walker, *Icarus* **48**, 150–166 (1981)
- R.P. Wayne, *Chemistry of Atmospheres* (Clarendon, Oxford, 1991)
- H.A. Weaver, P.D. Feldman, M.F. A'Hearn, C. Arpigny, J.C. Brandt, S.A. Stern, *Icarus* **141**, 1–12 (1999)
- M.S. Westley, R.A. Baragiola, R.E. Johnson, G.A. Barratta, *Planet. Space Sci.* **43**, 1311–1315 (1995)
- F.L. Whipple, W.F. Huebner, *Annu. Rev. Astron. Astrophys.* **14**, 143–172 (1976)
- J.K. Wilson, N.M. Schneider, *J. Geophys. Res.* **104**, 16567–16584 (1999)
- M.C. Wong, R.E. Johnson, *J. Geophys. Res.* **101**, 23243–23254 (1996)
- R.V. Yelle, J. Cui, I.C.F. Muller-Wodarg, *J. Geophys. Res.* (2008, in press)
- D.T. Young et al., *Science* **307**, 1262–1266 (2005)
- M.H.G. Zhang, J. Luhmann, S.W. Bougher, A. Nagy, *J. Geophys. Res.* **98**, 10,915 (1993)
- T.L. Zhang et al., *Nature* **450**, 654–656 (2007)
- J.F. Ziegler, J.P. Biersak, V. Littmark, *The Stopping and Range of Ions in Solids* (Pergamon, New York, 1985)